ISTANBUL TECHNICAL UNIVERSITY ★ GRADUATE SCHOOL OF SCIENCE ENGINEERING AND TECHNOLOGY

THEORETICAL, NUMERICAL and EXPERIMENTAL INVESTIGATION OF PARTIALLY COHERENT BEAM SHAPING

M.Sc. THESIS

Ceren ALTINGÖZ

Department of Physics Engineering

Physics Engineering Programme

DECEMBER 2015

ISTANBUL TECHNICAL UNIVERSITY ★ GRADUATE SCHOOL OF SCIENCE ENGINEERING AND TECHNOLOGY

THEORETICAL, NUMERICAL and EXPERIMENTAL INVESTIGATION OF PARTIALLY COHERENT BEAM SHAPING

M.Sc. THESIS

Ceren ALTINGÖZ
(509121126)

Department of Physics Engineering

Physics Engineering Programme

DECEMBER 2015

İSTANBUL TEKNİK ÜNİVERSİTESİ ★ FEN BİLİMLERİ ENSTİTÜSÜ

KISMİ EŞEVRELİ HÜZME ŞEKİLLENDİRİLMESİNİN TEORİK, NUMERİK ve DENEYSEL İNCELENMESİ

YÜKSEK LİSANS TEZİ

Ceren ALTINGÖZ
(509121126)

Fizik Mühendisliği Anabilim Dalı

Fizik Mühendisliği Programı

Tez Danışmanı: Doç. Dr. Selçuk AKTÜRK

ARALIK 2015

Ceren Altıngöz, a **M.Sc.** student of ITU **Graduate School of Science Engineering and Technology** with student ID 509121126 successfully defended the **thesis** entitled "**THEORETICAL, NUMERICAL and EXPERIMENTAL INVESTIGATION OF PARTIAL COHERENT BEAM SHAPING**", which she prepared after fulfilling the requirements specified in the associated legislations, before the jury whose signatures are below.

Thesis Advisor :	**Doç. Dr. Selçuk AKTÜRK** İstanbul Technical University	.....
Jury Members :	**Doç. Dr. Selçuk AKTÜRK** İstanbul Technical University	.....
	Yard. Doç. Alexandr JONAS İstanbul Technical University	.....
	Dr. Muhsin Eralp Koç University	.....

Date of Submission : 27 October 2015
Date of Defense : 22 December 2015

FOREWORD

I was an Industrial Product Designer working as Optics Engineer when I asked the question of what light was. All my aim was to understand the nature of light when I met my precious professor Selçuk Aktürk in 2013 at the entrance doors of physics department. Since then we have been working together and I have achieved to link my artistic background with the scientific technical side of optics. I am excessively gratefull to my professor for the patience and devotion he generously executed.

When working inside the optics group, I have met Berna Yalızay. I am also gratefull for her support when coping with hard subjects in Msc lectures. It was my pleasure to work with her through our experiments in the optics lab. I have completed my last experiments of SLM with Tansu Ersoy, I would also appreciate her support.

I would not forget to thank my dearest doctor Gülder Özkan for the support through the rough times, she is a unique personality.
I have my deepest thanks to my dearest mother as she cares us and my little daughter Duru in the most sincere way. Without her efforts, I would not be able to achive all.
I have the same deepest thanks for my dearest father. I will never forget how we managed to wake up in the darkest mornings when there is no sunshine at all, to catch the ship to the university.
I have my delicate thanks to my dearest brother and his pretty considerate wife, as they support me with kind attitudes.

I am totally gratefull to my little daughter Duru, for her existence in my life. I have already framed all the pictures she has drawn me. They helped me to work harder as she slept beside me.

All in one, I am happy to be the life long fellow of “lichttechnik”.

December 2015

Ceren ALTINGÖZ
(Optics R&D Engineer)

TABLE OF CONTENTS

Page

ABBREVIATIONS

NOL	**:** Nature of Light
SLM	**:** Spatial Light Modulator
LED	**:** Light Emitting Diode
TC	**:** Temporal Coherence
SC	**:** Spatial Coherence
SF	**:** Spatial Frequency
TF	**:** Temporal Frequency
LCD	**:** Liquid Crystal Displays
LCOS	**:** Liquid Crystal on Silicon (reflective LCD)
VAN	**:** Vertical-Aligned Nematic
PAN	**:** Parallel-Aligned Nematic
TN	**:** Twisted Nematic
DOC	**:** Degree of Coherence
EL	**:** Electroluminance
OASLM	**:** Optically Adressed Spatial Light Modulator
EASLM	**:** Electrically Adressed Spatial Light Modulator

LIST OF TABLES

Page

LIST OF FIGURES

Page

THEORETICAL, NUMERICAL and EXPERIMENTAL INVESTIGATION OF PARTIALLY COHERENT BEAM SHAPING

SUMMARY

What is Light? The answer to this simple looking conundrum still implies voids despite the new advancements in quantum field theory. Although light shows particle like nascency it propagates like waves. So the theory about the nature of light evolves into a composition of both particle and wave which is called “wave-particle duality”. As in this thesis, we try to investigate the propagation characteristics of light, we mainly focuse on the wave nature of it.

So the introduction part is written with the aim of giving theoretical background to construct the foundations of the experimental and numerical investigations that are coming in the next sections. In this sense, we opened the first subsection explaining the wave nature of light and its consequences like interference, diffraction and coherence theory. The subsection of coherence theory is divided into two, explaining the temporal and spatial coherence of light. We found it approciate to explain these two terms in separate sections as their relative importance have critical role on the diffraction patterns in our experimental findings.

Recent years are full of detailed papers with knowledge of the diffraction behaviour of coherent light sources, whereas studies researching diffraction with partially coherent, continous light sources were rare and there remains open points with unanswered questions. This is why in this thesis propagation dynamics of partial coherent light sources, the diffraction patterns that they produce and the possible beam shaping parameters of them are chosen to be studied.

We introduced the second section just to explain the coherent, partial coherent and incoherent light sources and their differences so that we would be clear when using them in our experiments and calculations. We used blue and white LEDs to represent partial coherent ligth sources in our experiments whereas used blue laser as coherent light source to compare our findings with partial coherent propagation dynamics.

We concluded the introduction part with a third subsection explaining the beam shaping techniques. Here we defined diffraction-free beams and then give detailed information about Bessel beams and Airy beams. As these two non-diffracting beams are the beams that we have generated through our experiments, it was also important for us to construct the theoretical background of them.

In the second main section by using all the gathered theoretical knowledge from the previous section, we started to numericaly model our partial coherent light source. As partial coherent ligth sources are the result of superposition of waves with different frequencies, we first focused on the superposition of waves. Then defined how we modeled the partial coherent light source in MATLAB. After introducing the diffraction integral, we put our previously modeled LED code into the diffraction integral to simulate our experiments done with LEDs. This has given us the chance to compare the simulated values and the experimented data. We concluded this section

by detecting the effects of the degree of coherence (of the input light source) on the diffracton pattern, transverse and longitudinal profiles of the beam.
The third main part is composed of the declarations of the experimental results done both with partial coherent and coherent light sources. We have performed each experiment both for “Bessel” and “Airy” beams. For each beam, experimental set up, experimental results and discussion part is composed.
We observed that “Bessel beams” are minimally affected by temporal coherence, while spatial coherence determines the longitudinal evolution of the beam profile. With spatially incoherent beams, the fringe contrast is comparable to the coherent case at the beginning of Bessel zone, while it completely fades away by propagation, turning into a cylindrical light pipe. Our results show that beam shaping methods can be extended to cases of limited spatial coherence, paving the way to new potential use and application of such sources. Experiments also has verified that our results are in accordance with the numerical calculations that we have performed at the second step.
Our realizations of “Airy beams” with the similar experiment set-up and same light sources, have proven that while airy beams can be easily generated by laser sources, the sharpness of the profile is lost when partial coherent blue and white LEDs are used.
So we decided to investigate further by using advanced beam shaping techniques in the fourth section. In order to do that we used SLM to give spatial phase to our partial coherent sources. We first calibrated the SLM and then calculated the required Bessel and Airy phase coefficients to use as a gray level input for the generation of each beam. We have concluded that although SLM is a more advanced technique to give phase to light, due to the partial coherent light sources’ special spatial phases optical elements like axicon and airy lens have given more clear beam profiles. To have more accurate results we concluded to scale the incoming beam for further studies.
The thesis is concluded by giving clarified answers to the open points with partial coherent light sources especially about their propagation characteristics. For further realizations possible new experimental techniques is also discussed. Our results show that spatially incoherent sources can be used in diffraction-free beam applications and depending on the particular goal, different longitudinal working planes could be selected to better serve the purpose. Moreover, the ability to modulate spatially incoherent beams also creates great potential to carve the outcoming beam accordingly, paving the way to the new potential use and application of such sources.

KISMİ EŞEVRELİ HÜZME ŞEKİLLENDİRİLMESİNİN TEORİK, NUMERİK ve DENEYSEL İNCELENMESİ

ÖZET

Işık nedir? Bu basit görünümlü bilmecenin cevabı kuantum alan teorisindeki birçok yeni gelişmelere rağmen hala bilinmeyenler içermektedir. Işık parçacık kökenli görülmesine rağmen dalgalar gibi yayınım gösterir. Böylece ışığın doğası üzerine kurulan teori, zamanla parçaçık ve dalga ikilemini birleştiren, "parçaçık-dalga çifti" ne dönüşmüştür. Bu tezde özellikle ışığın yayınım karakteristiği araştırıldığı için, dalga yapısı üzerine odaklanılmıştır.

Giriş bölümünde ışığın dalga yapısı ve bunun doğurduğu sonuçlar detaylı olarak işlenmiştir. Buradaki amaç takip eden bölümlerde anlatılan numerik ve deneysel bulguları yorumlamada temel oluşturacak bilgilerin toparlanması ve teorik bir altyapının oluşturulmasıdır. Bu anlamda ilk alt başlık doğadaki dalgalar ve bunların fiziğinin genel olarak incelenmesiyle başlar. Bu bölüm temel dalga yapısının kurulduğu ve bunun ışığın ilerlemesine benzeyen veya farklılıklar gösteren yönlerinin öne çıkarıldığı temel bilgiler içermektedir.

İlerleyen kısımlarda ışığın dalga modelini anlamakta temel iki olgu olan girişim ve kırınım anlatılmaktadır. Girişim ve kırınım olaylarının fiziği, bu olaylar arasındaki benzerlik ve farklılıklar belirtilerek; ışığın tüm bu fiziksel davranışlarının eşevrelilik teorisi ile bağlantıları kurulur.

Girişim ve kırınımın anlatıldığı bu bölümlerin hemen ardından eşevrelilik teorisine geçilmiştir. Eşevrelilik teorisi ile ilgili temel bilgileri takiben, ışığın zamansal ve uzaysal eşevrelilik tiplerinden detaylı olarak bahsedilmektedir. Bu iki terimi ayrı bir alt başlıkta incelemek istememizin sebebi deneylerimizdeki girişim desenleri üzerinde oluşturdukları etkilerin birbirlerine göre önemini anlamamızda çok önemli bir kaynak olacağı inancıdır.

Eşevreli ışık kaynaklarının kırınım davranışlarıyla ilgili bugüne kadar pek çok çalışma yapılmıştır, ancak yarı eşevreli hüzmelerin kırınım davranışlarıyla ilgili çalışmalar hem sayıca az hem de pek çok cevabı bilinmeyen açık noktalar içermektedir. Bu sebeple bu tezin, ışığın dalga yapısı altında özel olarak incelemeye değer gördüğü konu yarı eşevreli sürekli ışık kaynakları, bunların oluşturduğu kırınım desenleri ve bu kırınım desenlerini etkileyen parametrelerdir. Böylece bu özel alt başlık altında cevaplanmayı bekleyen pek çok soruya açıklık getirilmesi hedeflenmiştir.

İkinci ana bölümü eşevreli, yarı eşevreli ve eşevreli olmayan ışık kaynaklarını ve bunlar arasındaki farkları anlatmak için ayırdık. Işık kaynağı tipleri arasındaki farkların, yaptığımız deneylerimizde ve matematiksel hesaplarımızda büyük farklar oluşturduğunu görmemiz sebebiyle, bu bölümde kurulan teorik altyapının, sonuç bölümünde yapacağımız yorumlarda belirli bir netlik oluşturacağını düşündük.

Deneylerimizde yarı eşevreli ışık kaynaklarını temsil etmesi için mavi ve beyaz LEDleri, eşevreli ışık kaynağı olaraksa mavi lazeri kullandık.
Yaptığımız çalışmalarda lazeri kullanma amacımız, bu ışık kaynağının mükemmel eşevreli yapısı sebebiyle son derece net girişim desenleri vermesidir. Bu anlamda lazer ışık kaynağı kullanarak elde ettiğimiz sonuçları LED ile yaptığımız deneylerle karşılaştırma yaparak çıkarımlar yapmak için referans olarak kullandık.
Giriş bölümünü üçüncü bir son altbaşlıkla kapattık. Bu bölümde hüzme şekilllendirme yöntemlerinden ve deneylerimizde incelediğimiz iki kırınımsız ilerleyen hüzme şekli olan Bessel ve Airy hüzmelerinden bahsettik. Bölüme ışığın dalgalar şeklinde ilerlemesi sebebiyle, doğal olarak kırınıma uğrayacağı gerçeğine rağmen, bu hüzmelerin özel bir bölgede kırınımsız ilerlediklerini anlatarak başladık. Her iki hüzme şekli için kırınımsız ilerledikleri bu bölgeleri anlattıktan sonra, bahsettiğimiz Bessel ve Airy hüzmelerini ayrı ayrı alt başlıklarda inceledik. Deneylerimizde LEDlerin yayılım parametrelerini bu her iki hüzme ile de incelediğimizden, bu bölümün teorik alt yapısı da deney sonuçlarımız için yaptığımız yorumlarımızda önemli bir kaynak olmuştur.
Araştırmanın ikinci ana kısmında, giriş kısmında elde edilen tüm teorik bilginin de yardımıyla, hem kısmi eşevreli ışık kaynağını hem de yaptığımız deneyleri simule edecek şekilde modellediğimiz ışık kaynağının yayılımını modelledik. Kısmi eşevreli hüzmeleri modellemek için bir faz belirledik. Bu yarı eşevreli fazı oluşturuken eşevreli pek çok fazın toplanması metodunu kullandık. Bu sebeple önce dalgaların toplanması ilkesi üzerine yoğunlaştık.
Bir sonraki bölümde kırınım integralini, bir iğne deliğinden geçen ışık hüzmesinin belirlenen mesafede bir ölçüm ekranına ulaştığında nasıl bir elektromanyetik alan oluşturacağını hesaplayarak anlattık.
Ardından daha önce hesapladığımız kısmi eşevreli fazımızı kullanarak, hesapladığımız kırınım integraline exponansiyel olarak ilave ettik. Böylece LEDleri kullanarak yaptığımız deneyleri simule eder hale gelmiş olduk.
Bu bize deneysel bulgularımızla modellediğimiz numerik datayı karşılaştırma ve hangi parametreleri değiştiridiğimizde hangi değerlerin nasıl değiştiğini anlama olanağı verdi.
Bu bölümü kullanılan ışık kaynağının eşevrelilik derecelerini değiştirdiğimizde; girişim desenleri, dik ve yatay kesitteki ışık yayılımında oluşan etkileri inceleyerek tamamladık.
Üçüncü ana kısım eşevreli ve kısmi eşevreli ışık kaynakları ile yaptığımız deneyleri ve bunların sonuçlarını anlatmaktadır. Deneylerde giriş bölümünde teorisi anlatılan, Bessel ve Airy hüzmeleri üretilmiştir. Her hüzme için deneysel düzenek, deney bulguları ve elde edilen sonuçlardan çıkarımların yapıldığı tartışma bölümleri düzenlenmiştir.
Bulgularımız Bessel hüzmelerinin zamansal eşevrelilikten minimal şekilde etkilenmekle beraber uzaysal eşevreliliğin, hüzmenin ilerleme yönündeki profillerini önemli ölçüde etkilediği yönündedir. Kısmi eşevreli ışık kaynakları ile, Bessel hüzmesinin ilk kısımlarında saçakların görünürlüğü, eşevreli ışık kaynaklarınınki gibi nettir. Ancak hüzmenin ilerleyen kısımlarında görünürlüğün giderek düştüğü ve sonlara doğru silindirik bir yapıya dönüştüğü gözlemlenmiştir. Deney sonuçları hüzme şekillendirme yöntemlerinin belirli uzaysal eşevreli yöntemleriyle incelenebileceğini göstermiştir. Yaptığımız deneyler ile hesapladığımız kırınım desenlerinin ve dik hüzme profillerinin uyumu çalışmamızın doğruluğunu kanıtlamıştır.

Bessel hüzmeleri gibi Airy hüzmesini de kısmi eşevreli ışık kaynakları ile ürettiğimizde, laser ışık kaynağı ile kolayca üretilebilen bu hüzmenin kısmi eşevreli ışık kaynaklarıyla net bir biçimde üretilemediğini fark ettik. Bu bulgularımızı dikey kesit profilleri, CCD kameradan aldığımız görüntüler ve kaydettiğimiz görüntülerin maksimum yoğunluklarından hesaplattığımız MATLAB sapma grafikleriyle de raporladık.

Airy lens kullanarak yaptığımız bu deneylerde beklenen Airy profillerini görememiz sebebiyle SLM kullanarak ileri hüzme şekillendirme yöntemlerini deneme kararını aldık. Dördüncü bölümde bu doğrultuda yaptığımız deneyler ve elde ettiğimiz sonuçları aktardık. İleri hüzme şekillendirme deneylerini SLM adı verilen ve gelen ışığa istenilen uzaysal fazı eklemeye yarayan özel bir optik eleman kullanarak gerçekleştirdik. SLM, VGA görüntü ayrıştırıcısı ile laptopdan gelen siyah-beyaz görüntüyü içindeki LCD ekran ile uzaysal faz olarak, gelen ışık hüzmesine ekler.

CCD kamerada görüntülediğimiz hüzmenin elimizin hareketiyle dahi oluşan hava akımından belirgin ölçüde etkilendiğini gözlemledik, bu sebeple SLM'in kendi kalibrasyonu için detaylı çalıştık. Bu etap belirli bir gelen hüzmeye nasıl uzaysal faz farkı verildiğini anlamamızda da önemli bir adım oldu. Kalibrasyonu yaparken mavi lazeri kullandık. Bu ışık kaynağını kullanma sebebimiz eşevreli olması sebebiyle faz kaymasını iyi yakalayabilmemizdi. Kalibrasyonu yaparken faz değişimlerinin videolarını çektik ve videoları MATLAB'da işleyerek faz farkını incelediğimiz imajlara ve sonrada kaymaları saptadığımız grafiklere dönüştürdük. Bu bölüm programlama konusunda da becerilerimizi geliştirmemizi sağladı.

Bir sonraki adımda Bessel ve Airy hüzmelerini oluşturacak uzaysal faz farkını Matlab'da hesaplatarak; SLM'e bu faz farklarını VGA görüntü ayrıştırıcısıyla yansıttık.

Deneylerde önce mavi lazer ve mavi LED kullanarak Bessel hüzmelerini oluşturduk. Elde ettiğimiz sonuçlar mavi lazer için çok farklılık göstermemekle birlikte; mavi LED için axiconla elde ettiğimiz Bessel hüzme profillerinin, SLM ile elde ettiklerimize kıyasla daha net olduğunu tespit ettik. Benzer sonuçları Airy hüzmesini elde ettiğimiz deneylerimizde de bulduk.

SLM kullanılarak elde ettiğimiz Airy hüzme profilleri, lazer kullanarak yapılan deneylerdeki gibi net profiller çıkarmadı. Bunun sebeplerinden birinin SLM'in kendi geçirgen LCD ekranı sebebiyle gelen hüzmeye ayrıca bir uzaysal faz katması olarak düşünük. Bir diğer sebebin SLM'in düşük çözünürlüklü olması olabileceği kanısındayız.

Beklenilen netlikte hüzme profilleri oluşturabilmek için gelen hüzmenin büyütülüp eşevreliliğin daha yüksek tutulabileceği ve ilerleyen araştırmaların bu doğrultuda yapılabileceği fikrindeyiz.

Araştırmamızı kısmı eşevreli ışık kaynakları ve bunların yayılım özellikleri ile ilgili önemli bulguları sentezleyerek sonlandırdık. Elde ettiğimiz sonuçlar bize kısmı eşevreli ışık kaynaklarının kırınımsız ilerleyen hüzmelerin kullanılabileceği heryerde kullanılabileceğini göstermişir. Belirlenebilecek özel bir amaca göre bu hüzmelerin farklı yatay kesitlerde özel olarak şekillendirilebileceğini düşünüyoruz. İleri hüzme şekillendirme teknikleri her ne kadar beklediğimiz netlikte sonuçlar vermemiş olsa da uzaysal coheransı derinlemesine anlamamızda önemli bir adım olmuştur. SLM kullanarak gelen bir hüzmenin uzaysal eşevreliliğini değiştirip farklı profillerde pek çok hüzme yapılabileceği gerçeği, farklı amaçlar için hüzmelerin şekillendirilebileceğini göstermektedir. Bu sebeple uygun SLM seçimi ve optimum

gelen hüzme girdileriyle; bu ileri hüzme şekillendirme tekniklerinin de LED ışık kaynağı kullanılarak yapılacak ileriki çalışmalarda ümit vaad ettiğini görüyoruz.
Tüm bu çalışma, teorik, numerik ve deneysel boyutta tamamlandığından veriler, bulgular ve hesaplamaların birbirini tamamladığı kanısındayız.

1.INTRODUCTION

Understanding the nature of light has been the major interest of all researchers for ages. Prof Francesca Maria Grimaldi was the first to observe and note the phenomena of "Diffraction" [6]. Robert Hook was the first to observe colored interference patterns generated by thin films [7]. In 1845 Michael Faraday experimented an interrelationship between electric and magnetic fields and their relation to light. In 1873 James Clerk Maxwell (1831-1879) showed that an oscillating electrical circuit should radiate electromagnetic waves and he summarized all the extended empirical knowledge as $c = 1/\sqrt{\varepsilon_0 \mu_0}$. Einstein proposed photons as concentrated energy in small packets, giving the energy they radiate in terms of their frequency as $E = h\nu$. He was the first who suggest that the electromagnetic wave which we perceive macroscopically could be the statistical manifestation of a fundamentally granular underlying microscopic phenomenon that he called as photon [8]. So we may well comprehend propagation of light in the forms of waves whereas interaction of it with matter in the process of emission and absorbtion as in the forms of photons [6]. Light is neither wave nor a particle, but an intermadiate entity that obeys the superposition principle [9]. In the following subsections we will be giving information about the wave nature of light and its consequences.

1.1 Wave Nature of Light and Its Consequences

One may consider the essential feature of any wave existing in nature as its non-localization. Of what we should be understanding from this non-localization property is that, waves are travelling impulses in the medium, that they are not localized like particles.

A wave in this sense is the self sustaining disturbance of the medium through which it propagates. We call it a longitudinal wave if the medium is displaced in the direction of motion and a transverse wave if the medium is displaced in a direction perpendicular to that of motion.

Electromagnetic waves of light are transverse waves **[10].** The crest of a wave is the point on the medium that exhibits the maximum amount of positive or upward displacement from the rest position. The trough of a wave is the point on the medium that exhibits the maximum amount of negative or downward displacement from the rest position. The amplitude of a wave refers to the maximum amount of displacement of a particle on the medium from its rest position.

The wavelength of a wave is simply the length of one complete wave cycle. A wave is a repeating pattern. It repeats itself periodically over both time and space and the length of one such spatial repetition (known as a wave cycle) is the wavelength. The wavelength can be measured as the distance from crest to crest or from trough to trough. In the spatial domain, the localization of photons by photo detector makes it possible to define a "wave function" for the photon itself [9].These dynamics of wave function of light gives physical results called interference and diffraction that will be explained in the following sections.

1.1.1 Interference

One should have a clear understanding of the physical reaction under the colorful image of a soap to simply define what interference is. When an incoming ray of light strikes the outer surface of a bubble, part of the light ray is reflected immediately, while the other part is transmitted into the thin soap film. After reaching the inner surface of the film, this transmitted light ray is reflected back toward the outer surface. The light rays that are reflected off the inner surface of the bubble travel further than the light rays that are reflected off the outer surface. Some wavelengths will interfere destructively and others constructively, depending on the extra distance traveled by a transmitted-and-reflected ray. This distance depends on the angle of the incident light and the thickness of the film. This superposition of waves in and out of the soap buble is the reason for the interference of waves and so these interferences create colorful visible patterns on the buble.

Interference usually refers to the interaction of waves that are correlated or coherent with each other either because they come from the same source or because they have the same or nearly the same frequency. So in order to obtain interference, it is only necessary for the beams to possess statistical similarity in terms of the so-called

degree of coherence of light[11]. This is due to the reason if two beams are to interfere to produce a stable pattern, they must have very nearly the same frequency.

Interference can be observed with any kind of wave like light, radio, acoustic, surface water waves or matter waves. Interference patterns form when waves collide and during collisions the negative fields of the molecular electron shells oppose compression while converting the kinetic energy of the collision into potential energy of compressed fields [12]. In these patterns formed by converging trains of light waves, potential energy resides in the longitudinal, dark zones (null zones), kinetic energy in the parallel, bright zones. It is this kind of a mechanism that creates the constructive and destructive interferences in these waves. The amount by which such oscillators are out of phase with each other can be expressed in degrees from 0° to 360°. When the phase difference is 180 degrees (π radians), then the two oscillators are said to be in antiphase [13]. If two interacting waves meet at a point where they are in antiphase, then destructive interference will occur.

We should keep in mind that constructive or destructive interferences are limit cases and two waves always interfere, even if the result of the addition is complicated or not remarkable. On the other hand, the clearest patterns exist when the interfering waves have equal or nearly equal coherencies so the condition is that the light has to be coherent or at least partially coherent [14].

In this section we defined interference as the property of all types of waves to form characteristic stationary variations of the intensity by the superposition of two or more waves [15].Diffrcation on the other hand is an other phenemenon that includes the physics of interference and takes our interpretation to the one step further.

1.1.2 Diffraction

Diffraction is the result of interferences of wavefronts and it is the slight bending of light as it passes around the edge of an object [16].This behavior causes ripples at the boundaries of objects and diffraction is observed.

"Fresnel diffraction" refers usually to, although not exclusively, the phenomena observed close to a two-dimensional object illuminated by plane parallel incident light [13]. In this regard, we would see light to be bending around the edge of the object. The amount of observed bending depends on the relative size of the

wavelength of light to the size of the opening it passes. If the opening is much larger than the light's wavelength, the bending will be almost unnoticeable [17]. However, if the two are closer in size or equal, the amount of bending is considerable, and easily seen with the naked eye.

The main difference between interference and diffraction is the mechanism, diffraction involves a wave and some obstacle that bends the wave and intereference involves a wave that combine with other waves. In our experiments, both these phenomena happen and are part of the same overall phenomenon.

1.1.3 Coherence theory

Coherence of an optical field is understood as the ability of light to interfere**[18]**. Some features of the interference pattern provide a quantitative measure of the coherence between light vibrations at two points in space and at the two instants of time **[11]**.Coherence in this sense was originally realized with the experiments of Thomas Young and Michelson- Morley in optics**[19]**. Now it is used in any field that involves waves, such as acoustics, electrical engineering, neuroscience, and quantum mechanics as it is the basis for commercial applications such as holography, the Sagnac gyroscope, radio antenna arrays, optical coherence tomography and telescope interferometers like astronomical optical interferometers and radio telescopes.

This thesis is trying to find the answer to the question of what happens when two or more lightwaves overlap in some region of space in time when we use partially coherent light sources. So we take into account the fact, that, because of the finite extension of any physical source, and because of the finite spectral range of any radiation, coherent as well as incoherent superposition takes place side by side; the vibrations in the two beams will then be partially correlated, that one can say that the field is partially coherent**[20]**. For a clear exploration, we concern using light sources of both coherent and partially coherent, so that we have the chance to compare the results under differing conditions.

In wave mechanics, two or more wave sources are perfectly coherent if they have a constant phase difference and the same frequency. It is often convenient to divide coherence effects into two classifications as temporal and spatial [6]. Themporal coherence relates with the wavelength of the wave giving insight to coherence length

whereas spatial coherence relates with the transverse wavefront profile of the beam giving insight to coherence area. In the below sections, we will be giving further details of these two types of coherence.

1.1.3.1 Temporal coherence

Temporal coherence describes the correlation of a fixed point in a wave observed at different moments in time. Therefore, it gives an idea about the spectral bandwidth or in other word, wavelength of the light source that we use.

Observations in the Michelson–Morley experiment also give us an intuitive understanding about temporal coherence of a light source. By using a half transparent mirror D, in the middle of the set-up, the light source's incoming beam is splitted into two. One of the splitted beam's travelling distance is adjusted with the position of the moving mirror, M_2. Once both beams that are reflected from M_1 and M_2 interfere, the fringe pattern is observed on the screen. By sliding the movable mirror away from the screen gradually, the time, for the beam that is reflected from mirror M_2 to reach plane B is increases and so the fringes become dull and finally are lost **[19]**. The experimental set up showing temporal coherence can be seen in Figure 1.1 below.

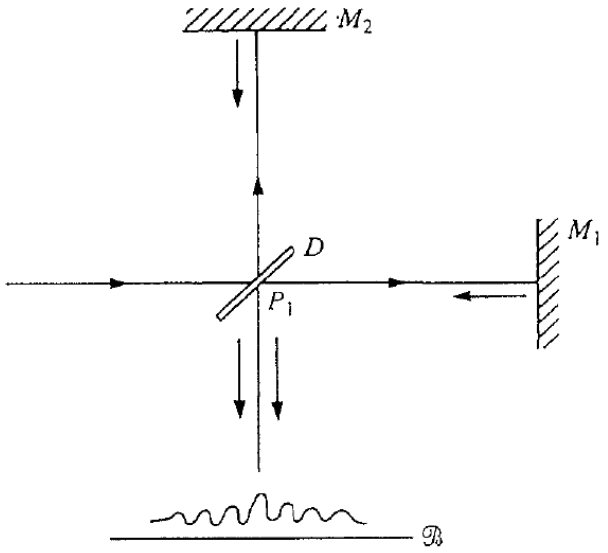

Figure 1.1: The movable mirror creates a phase shift between two waves and temporal coherence lenght of the light source is measured[1].

The appearance of the fringes is said to be a manifestation of temporal coherence between the two beams, because the contrast of the fringes depends on the time delay

Δt introduced between them**[11]**. We can observe the interference fringes only as long as:

$$\Delta t_c \leq \frac{1}{\Delta v} \tag{1.5}$$

where $\Delta \boldsymbol{v}$ is the bandwidth, and the time delay $\Delta \boldsymbol{t_c}$ is called the coherence time of the light and the corresponding path delay or more precisely the longitudinal coherence length of the light, $\Delta \boldsymbol{l}$ is:

$$\Delta l = \frac{c}{\Delta v} = \left(\frac{\bar{\lambda}}{\Delta \lambda}\right) \bar{\lambda} \tag{1.6}$$

$\bar{\boldsymbol{\lambda}}$ being the mean wavelength and $\Delta \boldsymbol{\lambda}$ the effective wavelength range. This quantity is called the coherence lenght of the light**[21]**.Temporal coherence tells us how monochromatic a source is. In other words, it characterizes how well a wave can interfere with itself at a different time. The coherence time shown as τ_c is the delay over which the phase or amplitude wanders by a significant amount and hence the correlation decreases by significant amount. At a delay of t=0 the degree of coherence is perfect, whereas it drops significantly as the delay passes $t=t_c$. Namely if Δt_c is large, the wave has a high degree of temporal coherence and vice versa**[8]**.

We define the term coherence length for the sources with varying frequencies to find the intervals where the source stays partially temporal coherent. The coherence length $\Delta \boldsymbol{l}$ then is the distance the wave travels in time $\Delta \boldsymbol{t_c}$ and the wave (e.g. an electromagnetic wave) maintains its degree of coherence the same in this specified interval.

As stated in equation 1.5, the larger the range of frequencies a wave contains, the faster the wave decorrelates and hence the smaller $\Delta \boldsymbol{t_c}$ is.

Therefore, we may conclude that a wave containing only a single frequency (monochromatic) is perfectly correlated with itself at all time delays, in accordance with the above relation conversely and a wave whose phase drifts quickly will have a short coherence time.

Sources like lasers have high monochromaticity that implies long coherence lengths up to hundreds of meters**[22]**. For example, a stabilized and monomode helium–neon laser can easily produce light with coherence lengths of 300 m, where as partial

temporal coherent sources as LEDs have less coherency lengths ranging from 10-100 μm.

1.1.3.2. Spatial coherence

Spatial coherence describes the correlation between different points of the same transverse wave profile in space at a fixed time. Therefore it gives an idea of spatial bandwidth. To define spatial coherence, let us consider two points P_1 and P_2 that at a time t = 0, they belong to the same wavefront so that the phase difference between their electric fields at time t = 0 is zero. If the difference $\phi_2(t)-\phi_1(t)$ of their phases also remains zero at times t > 0, we say that there is perfect spatial coherence between the two points P_1 and P_2**[15]**. Point sources like lasers are spatially coherent whereas extended sources like LEDs have partial spatial coherency. In practice, for any point P_1, in order to have some degree of phase correlation, point P_2 must lie within some finite area around P_1, which is called the coherence area. The high degree of spatial coherence of laser radiation stems again from the fact that the spatial field distribution of the beam generated by stimulated emission is a mode of the optical resonator**[23]**. On the other hand it is known that the interference fringes formed in a partially coherence light like LEDs are spatially localized**[24]**.

So basicly spatial coherence tells us how uniform the shape of the wave front is. The variation in the phase difference φ, results in a reduction in the contrast of the fringes. If the variations in φ, are sufficiently small, they may cause only negligible variations in the intensity so that there is spatial coherence. Large variations in φ can produce variations in intensity which are large enough for the contrast to fall almost to zero. The fringes are no longer visible, there is spatial incoherence. An intermediate case would indicate a degree of partial coherence**[18]**. To make the differences between spatial and temporal coherencies, respectively a transverse and an orthogonal section of a propagating wave can be examined as can be seen in Figure 1.2. In this frame spatial coherence gives us the correlation between the phases of a light wave for different points transverse to the direction of propagation at a fixed time.

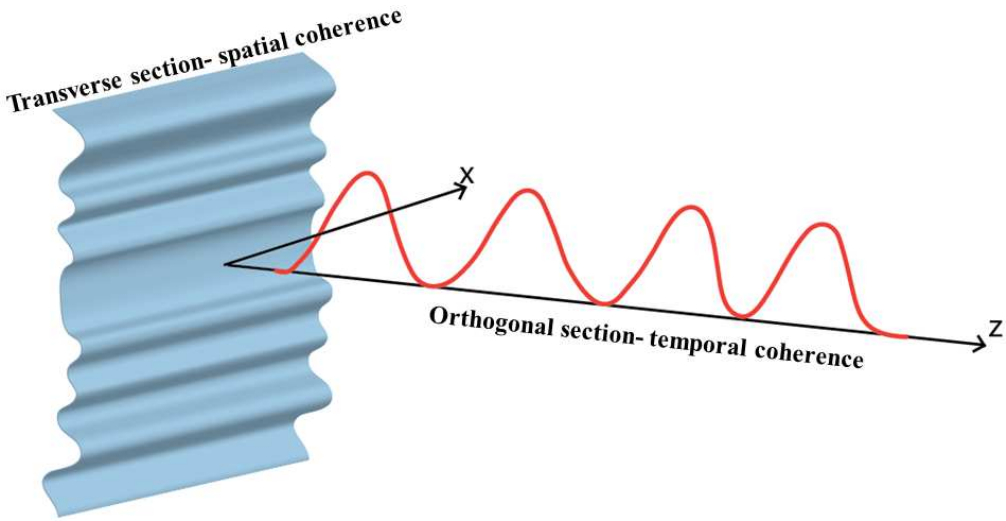

Figure 1.2: Schematics of spatial and temporal coherence.

When we examine these different points in a transverse section of a wave, we realize that the spatial coherency is high if they are in phase and it gets lower as the difference in phases increase. That is why spot kind of light sources like lasers have high spatial coherency but extended kinds like LEDs have partial spatial coherency**[22]**.In Young's double slit experiment if the space between the two slits is increased, the coherence dies gradually and finally the fringes disappear, proving the existence of spatial coherence. So this experiment provides information about the degree of spatial coherence, under conditions where a spatial seperation has been introduced **[20]**. Taking into account that σ is the light source having the form of a square of sides Δs and P_1 and P_2 are pinholes, we would expect to realize interference pattern on plane B only if:

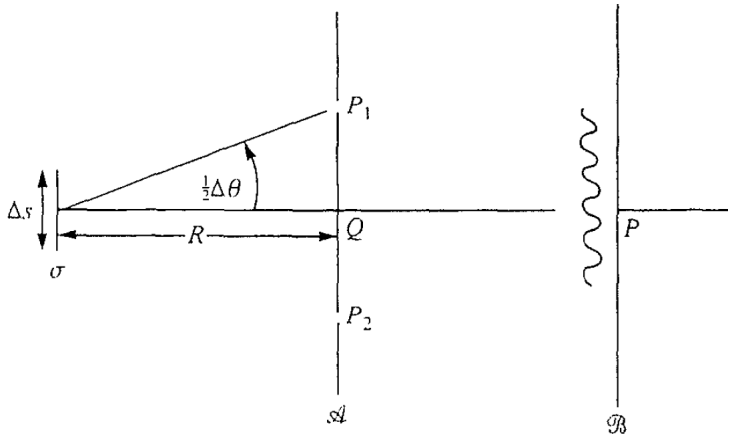

Figure 1.3: Schematics for understanding spatial coherence area[1].

$$\Delta\theta\Delta s \leq \bar{\lambda} \quad \textbf{(1.7)}$$

where $\boldsymbol{\Delta\theta}$ is the angle between P_1 and P_2 from the light source σ and $\bar{\boldsymbol{\lambda}}$ is the mean wavelength of the light. In order to observe fringes in the neighborhood of P, the two pinholes must be situtated within the coherence area $\boldsymbol{\Delta A}$:

$$\Delta A \sim (R\Delta\theta)^2 \sim \frac{R^2\bar{\lambda}^2}{S} \quad \textbf{(1.8)}$$

where $\boldsymbol{S = (\Delta s)^2}$ is the area of the source, R is the distance between th light source and plane A. Spatial coherence length is defined as the square-root of the coherence area**[1]**. If the spatial coherence length is less than the slit separation, then the relative phase of the light transmitted through each slit will vary randomly, washing out the fine-scale fringes, and a one-slit pattern will be observed. Young explained the interference pattern by considering the principle of superposition, and by measuring the distance between the fringes he calculated the wavelength**[2]**. On Figure 1.4 we can realize his ideation with a simple set up.

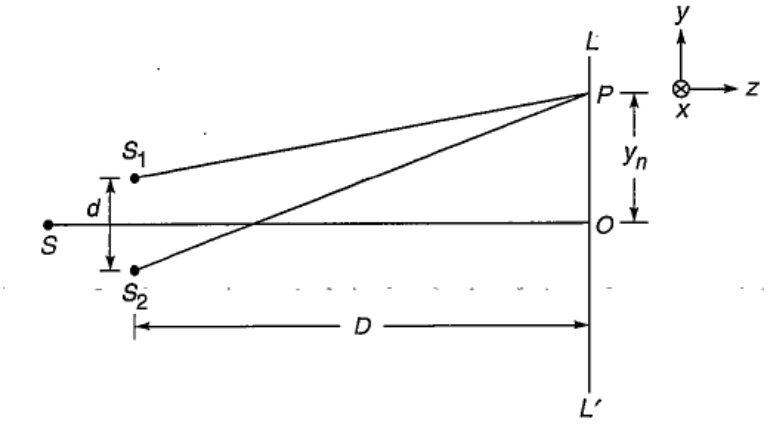

Figure 1.4: Schematics of an arrangement for producing Young's interference pattern[2].

Here S is the source whereas S_1 and S_2 represent the two pinholes, the interference pattern with dark and bright lines are seen on measure screen LL'. For any arbitrary point P on LL' to correspond to a maximum we must have:

$$S_2P - S_1P = n\lambda; n = 0,1,2,\ldots \quad \textbf{(1.7)}$$

As $S_1S_2 = d \; and \; OP = y_n$,

$$(S_2P)^2 - (S_1P)^2 = [D^2 + (y_n + d/2)^2] - [D^2 + (y_n - d/2)^2] = 2y_n d \quad (1.8)$$

Thus,

$$S_2P - S_1P = \frac{2y_n d}{S_1P + S_2P} \quad \textbf{(1.9)}$$

For d<<D then negligible error will be introduced when $\boldsymbol{S_2P + S_1P}$ is replaced by 2D. So we can consider;

$$S_2P - S_1P = \frac{y_n d}{D} \quad \textbf{(1.10)}$$

Using Equation (1.7) we obtain;

$$y_n = \frac{n\lambda D}{d} \quad \textbf{(1.11)}$$

Thus the dark and bright fringes are equally spaced and the distance between them is given by**[2]**;

$$\beta = y_{n+1} - y_n = \frac{(n+1)\lambda D}{d} - \frac{n\lambda D}{d} = \frac{\lambda D}{d} \quad \textbf{(1.12)}$$

which is the expression for the fringe width. The visibility of the fringes is decreased due to the increasing distance of the two pinoles**[18]**.

1.2 Light Sources

In this study types of light sources used in experiments and numerical calculations creates big differences in the results we experimented and verified as we mainly work on interference and diffraction affects.This is because with natural light from the sun or light from a bulb it is quite difficult to get interference effects, whereas it is no problem to obtain interference with the help of a laser [15]. For this reason we have given an importance to generate a separate section to define the main physical properties and the differences between the type of light sources. We have explained

coherent, incoherent and partial coherent light sources respectively so that we would be clear when comparing our experiment results with our numerical calculations and giving the reasons for our findings.

1.2.1 Coherent light sources (lasers)

In this section the fundamental physics behind laser operation will be introduced under three main subjects as spontaneous emission, stimulated emission and absorbtion. To describe the phenomenon spontaneous emission lets consider two energy levels where level 1 is the ground level and level 2 is the excited level. We can assume atoms at level 2 and as E_2>E_1, they will tend to decay to level 1 releasing the energy difference E_2-E_1. As can be seen on Figure 1.5 to the a), when this energy is delivered in the form of electromagnetic wave the process is called spontaneous (or radiative) emission**[25]**. As h is the Planck's constant, the frequency v_0 is then:

$$\nu_0 = \frac{\Delta E}{h} = \frac{E_2 - E_1}{h} \qquad \textbf{(1.13)}$$

Lets assume again that the atoms are initially in level 2 and an electromagnetic wave with frequency $\nu = \nu_0$is incident on the material as can be seen in Figure 1.5 to the b). In this case the energy difference is delivered in the form of an electromagnetic wave that adds to the incident wave, since the incoming wave's and material's atomic frequencies are the same. This is how stimulated emission occurs. The rate of stimulated emission is proportional to the population of the higher level[26].

The fundamental difference between spontaneous and stimulated emission is that, in spoantaneous emission the emitted atoms' phases have no certain relation with each other and emssion can occur in any direction; where as in stimulated emission the emission of any atom adds in phase to that of the incoming wave and they are in the same direction [27]. For the part c) of Figure 1.5, we can assume that the atom is initially lying in level 1 which we have previously defined as ground level.

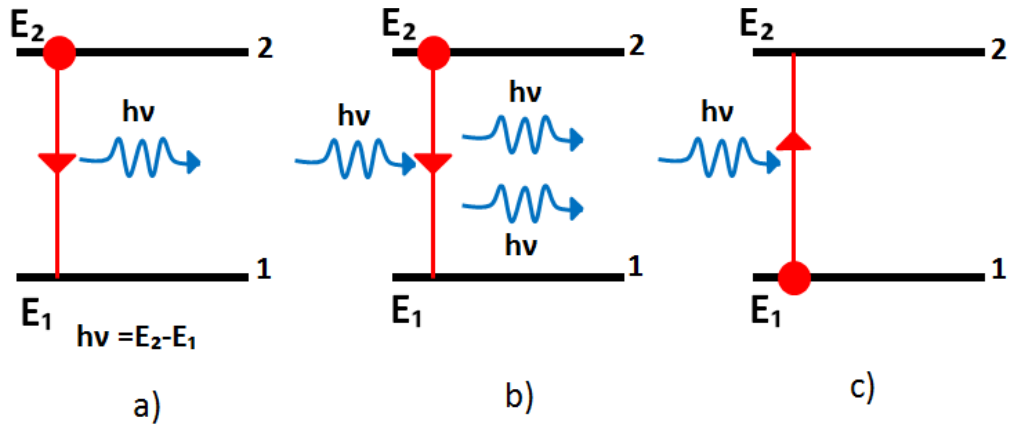

Figure1.5: Schematic illustration of three procceses: a) spontaneous emission, b) stimulated emission, c) absorbtion.

The atom will remain there unless a stimulus is applied. If an electromagnetic wave with frequency $\boldsymbol{\nu = \nu_0}$ is incident on the material, the atom will be raised to level 2. The energy difference to raise the atom to the level 2 is obtained from the energy of the incident electromagnetic wave and the process is defined as absorbtion**[27]**. Population inversion occurs when there are more atoms in the excited state than the ground state **[25]**. The reason of population inversion is the applied stimulation that pumps the atoms to the higher energy levels**[28]**. Once the critical inversion is achieved, oscillation starts from stimulated emission and lasing occurs**[25]**.

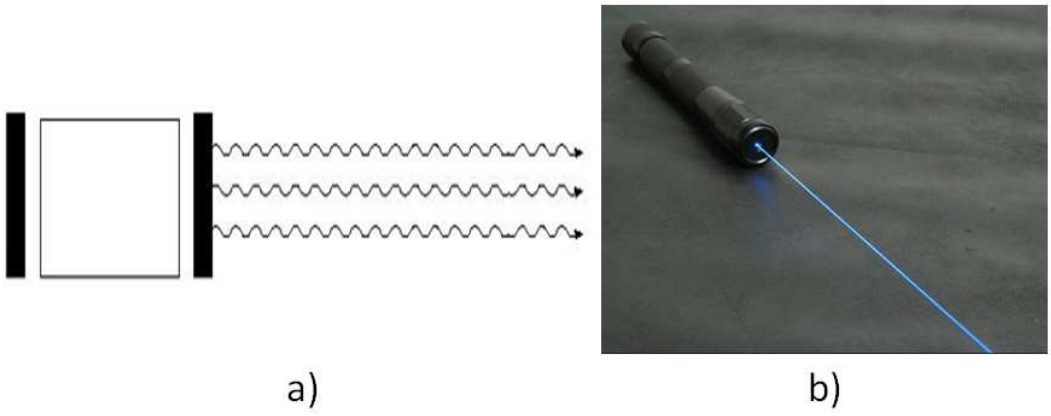

Figure1.6: a) Schematic of lasing b) laser radiation[3].

Laser radiation shows an extremely high degree of monochromaticity, coherence, directionality and brightness as compared to other noncoherent light sources[29].

1.2.2 Incoherent light sources (bulbs)

If the elements of an object emit entirely incoherent vibrations, which are independent of one another, the radiation emitted by this object is said to be incoherent. The sun, the stars, the planets, landscapes and the various monochromatic radiations forming the spectrum of a source, are all examples of incoherent objects **[18]**. A good example to the incoherent light sources could be considered as most of the filamanted light bulbs, which may well be named as incandescent lamps. These light sources emit light with a wire filament, heated to a high temperature by the electric current passing through it **[29]**. The metal wire is mounted in the glass bulb filled with an inert gas**[22]**. This procedure of producing light is simply the black body radiation of the filament under high temperature. In fact, we can be much more precise: a body emits radiation at a given temperature and frequency exactly as well as it absorbs the same radiation**[30]**. Due to this type of radiation, light waves are distributed in each direction randomly. Hence the comparison of the angular distribution of radiation from the two sources (lasers and bulbs) seems to indicate that there must be a close connection between the state of coherence of a source and the distribution of the radiant intensity of the light that the source generates**[20]**. Figure 1.7 below shows the section and the radiation of such light source.

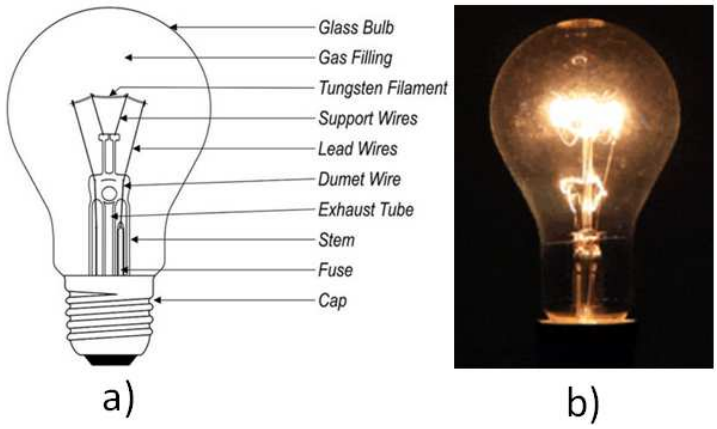

Figure1.7: a) Schematic filament bulb, b) Its incoherent radiation[31].

We have shortly examined the incoherent light sources to give intuitive insights to the understanding of partial coherent light sources.

1.2.3 Partially coherent light sources (light emitting diodes)

Thus far in explanations of phenomena involving the superposition of waves, we've restricted the treatment to that of either completely coherent or completely incoherent disturbances, however there is a middle ground between these antithetic poles, which is of considerable contemporary concern and it is partial coherence[8]. A good example of the partially coherent light sources would be light-emitting diodes (LEDs) that found broad application fields in industry. LEDs are also promising for scientific experiments as they exhibit characteristics between lasers and bulbs.

Understanding the propagation characteristics of LEDs is the core purpose of this thesis. In such solid-state light sources the electric current is converted into light by recombination of excited states of atoms into the ground state via emission of a photon[15]. LEDs are fabricated from semiconductor materials in which a p/n junction is fabricated[32].The nature of the excited state may differ for different types of electroluminescence (EL). Electroluminescence is a non-thermal generation of light resulting from the application of an electric field to a substance[33]. It differs from thermal radiation (incandescence) in the relatively narrow range of wavelengths contained within its spectrum which is typically 5 to 20 nm[34].

EL in general describes the direct recombination of electrons and holes in a suitable semiconductor structure[15]. Under forward bias conditions, electrons are injected into the p-type semiconductor and holes are injected into the n-type material. Recombination of these minority carriers with the majority carriers at the p/n junction results in near bandgap radiation[34] So at the depletion zone electrons fills the holes and light is emitted. The released photon energy is approximately equal to the bandgap energy of the semiconductor [20].

In most conventional LEDs, the light emiting semi-conductor material is inorganic, and InGan is an efficient, frequently used example with a band-gap of 1.37 eV. It was in 1993 when Nakamura et al. achieved the breakthrough for solidstate lighting by proving the successful use of InGaN as a material in blue LEDs [36]. The wavelength of the emitted light is governed by the energy bandgap of the semiconductor material, and is given as[32]:

$$\lambda = \frac{1.24}{E_{gap}}[\mu m] \quad \textbf{(1.14)}$$

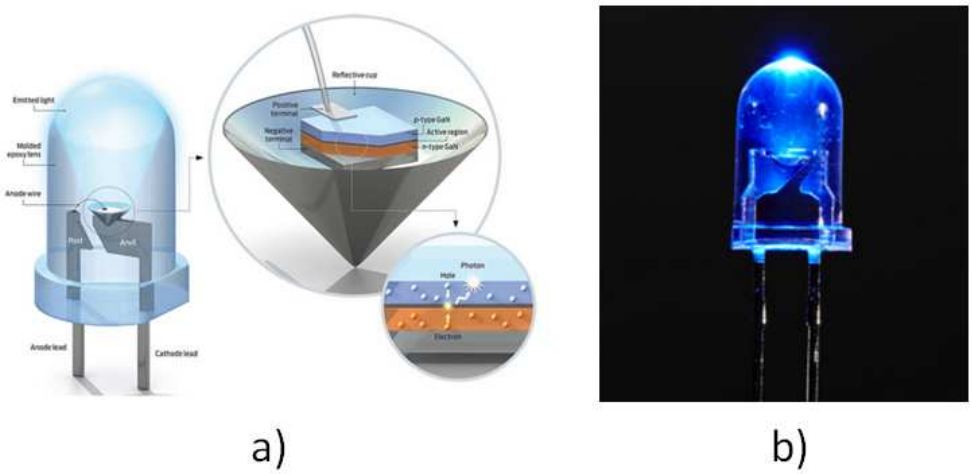

Figure 1.8: a) Schematics of LED, b) blue LED radiation[4].

The schematics structure for a blue LED and the radiation of it can be seen in the Figure 1.8. Partially coherent sources stay in the middle of coherent and incoherent counterparts. We accept two wave sources to be perfectly coherent if they have a constant phase difference and the same frequency.This ideal property of waves enables stationary (temporally and spatially constant) interference. In the following section, we will further investigate coherence theory with its spatial and temporal components to fix our understanding over partial coherent light sources.

1.2.4 Types of the light sources used in our experiments

In this section, we describe the coherence properties of light sources used in our experiments. The light sources are blue LED, white LED and laser diode respectively. We have summarized light sources according to their central wavelength, emitter area, viewing angle, current voltage via amper and temporal coherence length properties.

As can be seen in Table 1.1, the blue LED does not have spatial coherence but has limited temporal coherence, whereas white LED has neither spatial nor temporal coherence, lasers in this sense have both temporal and spatial coherence that we used them as a concrete source for comparison.

Table 1.1: Type of the light sources that are used in our experiments.

			
	BLUE LED	WHITE LED	LASER DIODE
Central Wavelenght	465nm	400-750 nm	633nm
Emitter Area	0,4 mm²	0,8 mm²	collimated, point like.
Viewing Angle	±8°	±15°	*
Current Voltage via Amper	at 2.5 V- 1mA	at 3 V- 380mA	at 5,2V- 50mA
Temporal Coherence Length	100µm	*	2m

1.3 Beam Shaping

1.3.1 Diffraction-free propagation

As diffraction is a fundamental part of light, imagining non-diffracting beams seems ridicilous, but these beams do exist . This is why “Diffraction-free propagation” is an important title that we want to fill under before directly passing to the explanations of Bessel and Airy beams. Diffraction free beam is invariant with respect to diffraction from one plane to the next[37]. Of course, it is not possible for a beam passing through a finite aperture to avoid diffraction.

Durnin has recently pointed out that the Helmotz equation has a class of diffraction-free mode solutions[38]. So these beams are theoretically non diffractive propagating and in reality they are only non-diffracting in their diffraction-free zone. We consider the diffraction-free zone within the distance (z_{max}), these beams remain their properties the same as can be seen in Figure 1.9 which is painted to red.

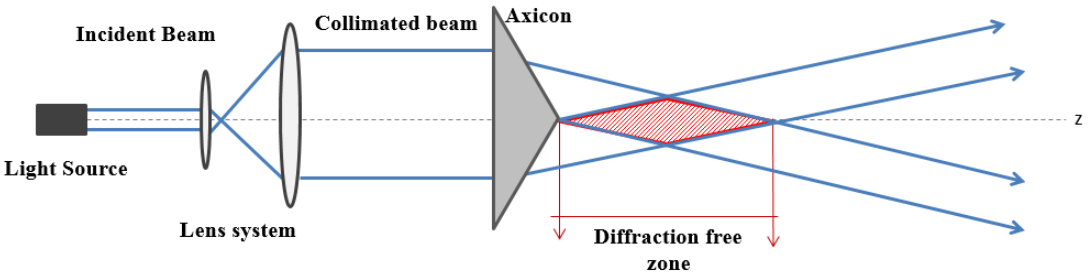

Figure 1.9: Diffraction-free zone.

So when investigating the properties of Bessel and Airy beams it should be clear for us that they can be observed by the diffraction of the light source we used in our

experiments and they don't diffract during their propagation at their own diffraction-free zone.

In the following sections we will be investigating Bessel and Airy beams respectively, so that we would have gathered all the theoretical knowledge we would need for interpreting our numerical and experimental findings in the conclusion part.

1.3.2 Bessel beams

Perhaps the best known example of such a 2D diffraction-free optical wave is the so-called Bessel beam first suggested and observed by Durnin et al. [39]. This work sparkled considerable theoretical and experimental activity and paved the way toward the discovery of other interesting nondiffracting solutions. A Bessel beam gets its name from the description of such a beam using a Bessel function, and this leads to a predicted cross-sectional profile of a set of concentric rings[40].The Bessel beam with a transverse section on the left and its line profile on the right can be seen in Figure 1.10.

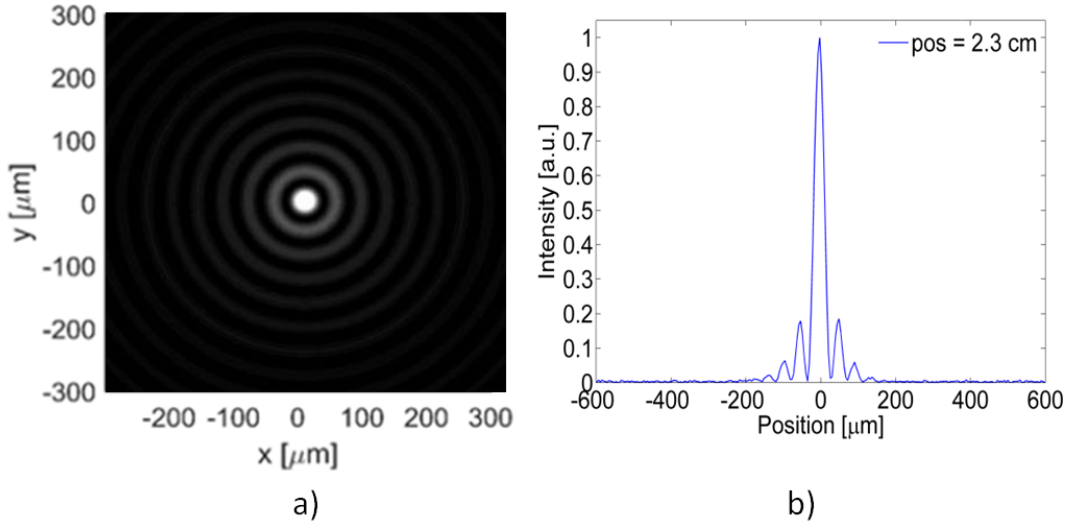

Figure 1.10: Bessel beam a) transverse section, b) its line profile .

Bessel beams are diffraction-free (propagation-independent) solutions of Helmholtz equation[38]. In cylindrical coordinates the electric field envelopes of Bessel beam follow the form [39]

$$E(r,\phi,z) = E_0 exp(ik_z z) J_n(k_r r) exp(\pm in\phi) \qquad \textbf{(1.15)}$$

where J_n is the *n*-th order Bessel function of the first kind, k_z and k_r are longitudinal and radial wave-vector components. In the lowest-order case of *n = 0*, the radial intensity profile appears as a bright spot surrounded by concentric rings of decreasing amplitude. Beams described by higher order Bessel functions (n>0), the High-Order Bessel Beams, have a phase singularity on the beam axis and hence have a non-diffracting dark, rather than bright core[41]. The associated intensity of zero-order Bessel beam is given by:

$$I \propto | J_0(k_r r) |^2 \qquad \textbf{(1.16)}$$

Equation 1.16 is independent of the coordinates, which means that the intensity profile of an ideal Bessel beam does not change under free space propagation. This means that there is no change in the cross-section as the beam propagates and thus the beam can be considered diffraction free, or propagation invariant[40]. These ideal Bessel beams should carry infinite energy; therefore, they cannot be generated experimentally. However, approximations to such idealized beam can be obtained over a limited spatial range, by using various methods, of which axicon focusing is by far the most common [22],[43].

Diffraction-free Bessel beams of 0^{th} order are obtained by the superposing of plane waves whose wave vectors make an angle with the propagation axis. These plane waves are realized with point sources that are distributed uniformly around a circle and an infinitely large aperture lens. After the field passes through the lens it has non diffracting properties and is described by the zero-order Bessel function. The beam is diffraction free within only a limited region. The beam generated from such a geometry is referred to as a quasi-diffraction-free beam. And bessel beams propagate in such a quasi-diffraction-free manner exhibiting lines of foci much longer than the Rayleigh distances of focused Gaussian beams[39]. A Bessel-like beam can be easily formed by passing a Gaussian laser beam through an Axicon [44]. The Axicon is a specialized type of lens which has a conical surface. Unlike a converging lens which is designed to focus a light source along the optical axis, the design of an Axicon focuses a light source to a line consisting of multiple points along the optical axis[45]. So a beam generated by an Axicon crosses the optical axis and forms rings of increasing diameter with constant ring thicknesses generating 0^{th} order Bessel beams which have a high intensity on the center and smaller fringes on the sides. It is important to note that the Bessel beam has its energy evenly distributed between its

rings, so the more rings the beam has, the lower the energy in the central core [46]. One other important property of Bessel beams is their ability to reconstruct even if they hit an obstruct. After some distance beyond the obstacle, the outer lobes of the Bessel beam act to replenish the central maximum and thus the beam is reconstructed[47]. This reconstruction is due to the conical wavefronts of the Bessel beams.

A Gaussian beam passing through an axicon gains a phase shift depending on the maximum radius of the input field "r". This phase shift can be respresented in terms of the wave vector "k", axicon tip degree "γ" and refraction index "n" of the axicon as[44]:

$$\phi(r) = kr\ tan\gamma(1-n) \quad \textbf{(1.17)}$$

As for small γ values, $\tan\gamma \cong \gamma$ the equation 1.18 can be simplified to:

$$\phi(r) = kr\ \gamma(1-n) \quad \textbf{(1.18)}$$

We can define the Bessel beam half cone angle after axicon as:

$$\beta = \text{asin}(nsin\gamma) - \gamma \cong (n-1)\gamma \quad \textbf{(1.19)}$$

As the wave vector on the r direction is k_r, we can write it as:

$$k_r = ksin\beta \cong k\beta = k(n-1)\gamma \quad \textbf{(1.20)}$$

So the spatial phase shift due to the axicon can be summarized as :

$$\phi(r) = -k_r r \quad \textbf{(1.21)}$$

The diameter of the central lobe (distance between the first two zeros) is given by[48]:

$$d_{cent} = 0.7655\frac{\lambda}{sin\beta} \quad \textbf{(1.22)}$$

When the input beam is Gaussian-shaped, the depth of the Bessel zone is approximately given by[48]:

$$z_{max} = \frac{k}{k_r} w_0 \quad \textbf{(1.23)}$$

where w_0 is the spot size of the incident Gaussian beam.

As is explained in detail in the Fresnel diffraction of Equation 2.22, the phase shift generated by the axicon is added to this diffracted wave equation as an exponential coefficient.

$$E(r,z) \propto \int \exp\left(\frac{-r'^2}{{w_0}^2}\right).exp\left(ik\frac{r'^2}{2z}\right) .\exp(-ik_r r)J_0(\frac{krr'}{z})r'dr' \quad \textbf{(1.24)}$$

By applying stable phase approach to the integral [42],

$$I(r,z) \cong \frac{4k_r P}{w_0}\frac{z}{z_{max}}{J_0}^2(k_r r)\exp(-\frac{2z^2}{{z_{max}}^2}) \quad \textbf{(1.25)}$$

Here P is the total power of the beam, w_0 is the waist spot size, z is the longitudinal position and $z_{max}=w_0/\tan\beta$ is the position where the axial intensity is measured to be maximum.

Plane waves of incoming Gaussian beam, propagating parallel to propagation axis pass through the axicon and refracted. The diffracted plane waves coming from the upper and lower zones of the axicon, have constructive and destructive interference with each other that when they hit the measure screen we realize the Bessel beam profile. This is also what we experiment when creating Airy beams however there is a few steps more and we use Airy lens instead of axicon.

1.3.3 Airy Beams

It was Berry and Balazs whose calculations proved that Airy wave packet was a solution to the Schrödinger equation[50]. Siviloglou et al. in 2007 experimentally showed that Airy beams also propagate diffraction-free[51]. Similar to Bessel beams, Airy beam intensity also stays high over much longer distances than conventionally focused Gaussian beams. Differently from Bessel beams, however, Airy beams also exhibit acceleration[52].

Gaussian laser beams can be converted to Airy–Gauss beams by introduction of cubic spatial phase followed by optical Fourier transform with a convex lens[53].

To examine the behavior of optical Airy wave packets, potential-free Schrödinger equation is taken into account [54]:

$$i\frac{\partial ø}{\partial \xi} + \frac{1}{2}\frac{\partial^2 ø}{\partial s^2} = 0 \quad \textbf{(1.26)}$$

where ø is the electric field envelope, $s = x/x_0$ represents a dimensionless transverse coordinate, x_0 is an arbitrary transverse scale, $\xi = z/k(x_0)^2$ is a normalized propagation distance, and $k= 2\pi n/\lambda_0$[52]. So Equation 1.26 admits the following Airy nondispersive solution:

$$\phi(\xi, s) = Ai(s - \left(\frac{\xi}{2}\right)^2)\exp(i\left(\frac{s\xi}{2}\right) - i\left(\frac{\xi^3}{12}\right)) \quad \textbf{(1.27)}$$

At the origin $\phi(0, s) = Ai(s)$. Equation 1.27 clearly shows that the intensity profile of this wave remains invariant during propagation while it experiences constant acceleration. The term $(\xi/2)^2$ in the same equation describes this ballistic trajectory. Figure 1.11 depicts the characteristic ballistic trajectory of Airy beam propagation.

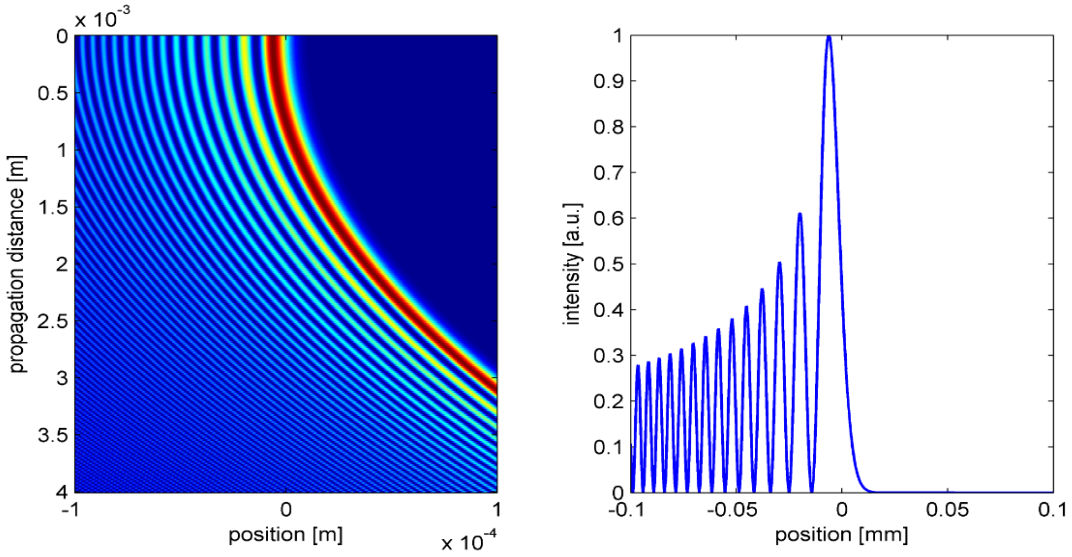

Figure 1.11: Airy beam a) transverse section, b) its line profile.

We can see that both Bessel beams and Airy beams are formed due to the fact of diffraction and they stay diffraction-free for a certain distance where they show their individual propagation characteristics.

The deflection of the Airy beam can be calculated with the formula seen below.

$$X_d = \theta z + \frac{z^2}{(4k^2 {x_0}^3)} \quad \textbf{(1.28)}$$

One last property of Airy beams is that they self-heal themselves during propagation. Siviloglu et al. have experimantally proved that even the main lobe on upper right corner of Airy beam is blocked, it reconstruct itself[55]. This property cause the beam to be also robust in adverse environments such as in scattering and turbulent media.

In the following section we will be giving numerical calculations for the theoretical background we have constructed. By this way we would be exploring the properties of the spatially incoherent light sources.

2.NUMERICAL ANALYSIS of DIFFRACTION INTEGRAL

2.1. The Superposition of Waves

All interference and diffraction phenomena that we observe when investigating the nature of light is the result of the fact called “superposition of waves”. Basicly when talking about superposition of waves we mainly are interested with what happens when two or more lightwaves overlap in some region of space and how the specific properties of each constituent wave (amplitude, phase, frequency, etc.) influence the ultimate form of the composite disturbance.

When we consider an electromagnetic light field with electronic and magnetic components at each three dimensions as E_x, E_y, E_z, B_x, B_y and B_z we can realize that they satisfiy the scalar three dimensional wave equation as:

$$\frac{d^2\psi}{dx^2} + \frac{d^2\psi}{dy^2} + \frac{d^2\psi}{dz^2} = \frac{1}{v^2}\frac{d^2\psi}{dt^2} \qquad \textbf{(2.1)}$$

As a means for obtaining the intensities of diffracted beams of radiation, we make use of the convenient conventional idea of a wave function.**[13]**As any linear combination of $\psi(\vec{r}, t)$ can be a solution to the above wave equation, we can define a general solution where the coefficients C_i are simply arbitrary constants, as:

$$\psi(\vec{r}, t) = \sum_{i=1}^{n} C_i \psi_i(\vec{r}, t) \qquad \textbf{(2.2)}$$

Known as the Principle of Superposition, this equation clarifies that the physics of the resultant disturbance at any point in a medium is the algebraic sum of the separate constituent waves.

If we try to write the physical background of the addition of two waves, we can write wave 1 as one of the solutions of $\psi(\vec{r}, t)$:

$$E_1 = E_{01} sin(wt + \alpha_1) \qquad \textbf{(2.3)}$$

and wave 2 as:

$$E_2 = E_{02} sin(wt + \alpha_2) \quad \textbf{(2.4)}$$

Here we should note that "E_0" is the amplitude, "$\boldsymbol{w}$" is the frequency, "t" is time and "α" is the phase representatives of our waves.

The total disturbance would then be:

$$E = E_0 sin(wt + \alpha) = E_1 + E_2$$

$$E = E_{01}(sin\, wt\, .\, cos\alpha_1 + coswt.\, sin\alpha_1) + E_{02}(sin\, wt\, .\, cos\alpha_2 + coswt.\, sin\alpha_2) \quad \textbf{(2.5)}$$

where;

$$E_0 cos\alpha = E_{01}\, cos\alpha_1 + E_{02}\, cos\alpha_2 \quad \textbf{(2.6)}$$

$$E_0 sin\alpha = E_{01}\, sin\alpha_1 + E_{02}\, sin\alpha_2 \quad \textbf{(2.7)}$$

therefore:

$$(E_0)^2 = (E_{01})^2 + (E_{02})^2 + 2E_{01}E_{02}\, cos(\alpha_2 - \alpha_1) \quad \textbf{(2.8)}$$

which gives a nice solution for the amplitude of our composite wave. And to get the phase $\boldsymbol{\alpha}$, we can just divide equation 2.6 with equation 2.7, as:

$$tan\alpha = \frac{E_{01}\, sin\alpha_1 + E_{02}\, sin\alpha_2}{E_{01}\, cos\alpha_1 + E_{02}\, cos\alpha_2} \quad \textbf{(2.9)}$$

So then we have written the composite wave equation from two wave disturbances and see from the resultant wave that although the frequency stays the same, the amplitude and phase do changes.

As the flux density of a lightwave is proportional to its amplitude squared, we can read from Equation 2.8 that there is an extra term to that of the square of the component waves, which we can write as: $2E_{01}E_{02}\, cos(\alpha_2 - \alpha_1)$. This additional term in the equation is what we call the interference term.

What has a big impact on the interference pattern is the difference between phases of component waves as, $\delta = \alpha_2 - \alpha_1$. This phase difference may both be caused of the difference in path lenght due to medium they travel or cause of the initial phase differences of the two waves themselves. We can write the equation of this expression as follows:

$$\delta = (kx_1 + \alpha_1) - (kx_2 + \alpha_2) = \frac{2\pi}{\lambda}(x_1 - x_2) + (\alpha_1 - \alpha_2) \quad \textbf{(2.10)}$$

where x_1 and x_2 are the distances from the light source to the observation point, λ is the wavelength in the pervading medium, α_1 and α_2 are initial own phases of the light waves. Here we should note that we could modify our equation considering that waves may travel different medias before arriving the observation point. So that it should be an asset to define the index of refraction, $\boldsymbol{n} = \frac{\boldsymbol{\lambda}}{\boldsymbol{\lambda_0}}$. δ is then:

$$\delta = \frac{2\pi}{\lambda_0} n(x_1 - x_2) + (\alpha_1 - \alpha_2) \quad \textbf{(2.11)}$$

where $k_0 = \frac{2\pi}{\lambda_0}$ is the propagation number of the waves travelling in the vacuum and $\Lambda = n(x_1 - x_2)$ is the optical path difference. The important thing at this step is to construct the spatial and temporal coherence frames with their components correctly. Henceforth, the symbols k and λ will be reserved for the light wave itself whereas κ and ϰ to describe spatialoptical patterns**[8]**. The wavelength λ and and the wave number k are the terms which define directly temporal coherence of the light source. They are the properties of longitudinal distribution of light across space as can be seen with red lines at Figure 2.1. However when we consider spatial frequency we should imagine the transverse wave profiles to define spatial properties of the light wave at a certain time. Spatial peridocitiy ϰ and spatial wave number κ define spatial optical patterns of the light wave as can be seen on blue transverse plane at Figure 2.1.

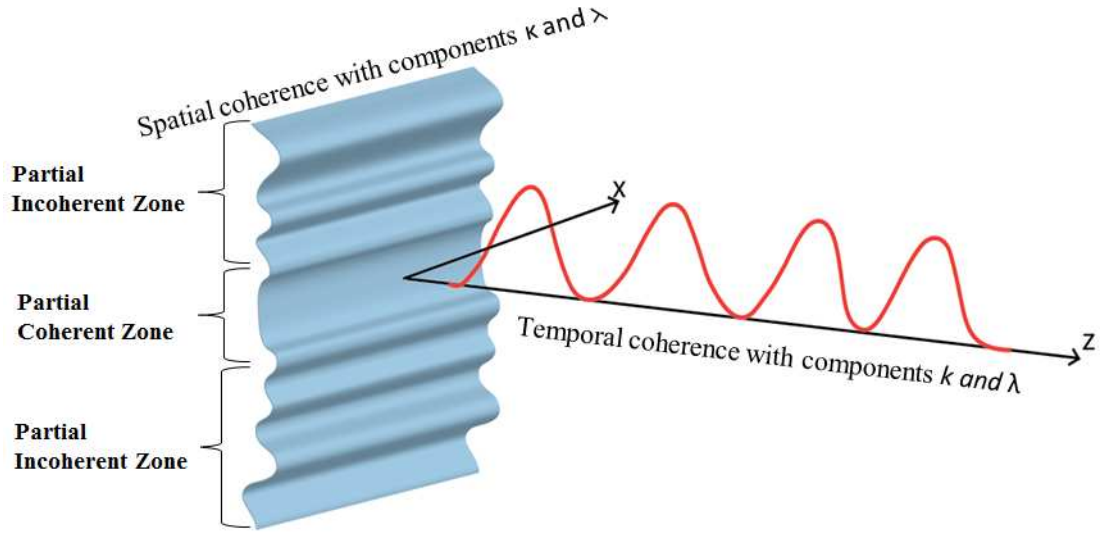

Figure 2.1: Spatial coherence with components κ and ϰ, temporal coherene with components *k* and λ.

In order to model spatial coherence properties below, we introduce spatial periodicities, at integer fractions of a defined width w0. If we divide a certain spatial width of W_0, by any integer N, we will obtain the spatial periodicty ⋋, as:

$$⋋ = \frac{W_0}{N} \tag{2.12}$$

It is important to note that the spatial periodicty of any wave would decrease by increasing the integer N that is chosen. In our model we have chosen N to be 10. So that we would start to see a more spatially incoherent distribution on the blue plane.

In order to make a certain beam profile spatially incoherent, we add several ⋋'s with arbitrary phase relations. For the spatial wave number κ, we can consider the following equation as:

$$\kappa = \frac{2\pi}{⋋} \tag{2.13}$$

The vibration emitted by a source at a given instant is the sum of the individual vibrations due to the different atoms[18]. So just as investigated in the beginning of this section with superposition of waves, we will consider the same logic of addition to construct the partial coherent phase that will be exponentially added to our final diffraction equation. To do so the basic solution for a wave propagating along the same direction is introduced as:

$$\varphi_i = A_i sin(k\kappa_i r + \alpha_i) \tag{2.14}$$

To define the partially coherent spatial phase, we would then get total φ and obtain $\boldsymbol{\varphi_{incoh}}$ as:

$$\varphi_{incoh} = \sum_{i=1}^{n} \varphi_i \tag{2.15}$$

2.2. Diffraction Integral

In the previous section we have modeled our spatially partial coherent light source. In the experimental set up the light from the source passes through a pinhole where it exhibits diffraction and then it is conveyed to the axicon where it gains an extra spatial phase. In the first part of this section, we are mainly interested in the calculations of what happens to the incident light wawe-fronts after they pass from the circular aperture of the pinhole. So we ask the question of what is E(x, y) at a distance z from the plane of aperture is.

We imagine a set up as can be seen in Figure 2.2 to calculate the formulations of diffraction from a circular aperture of a partial spatial coherent light source.

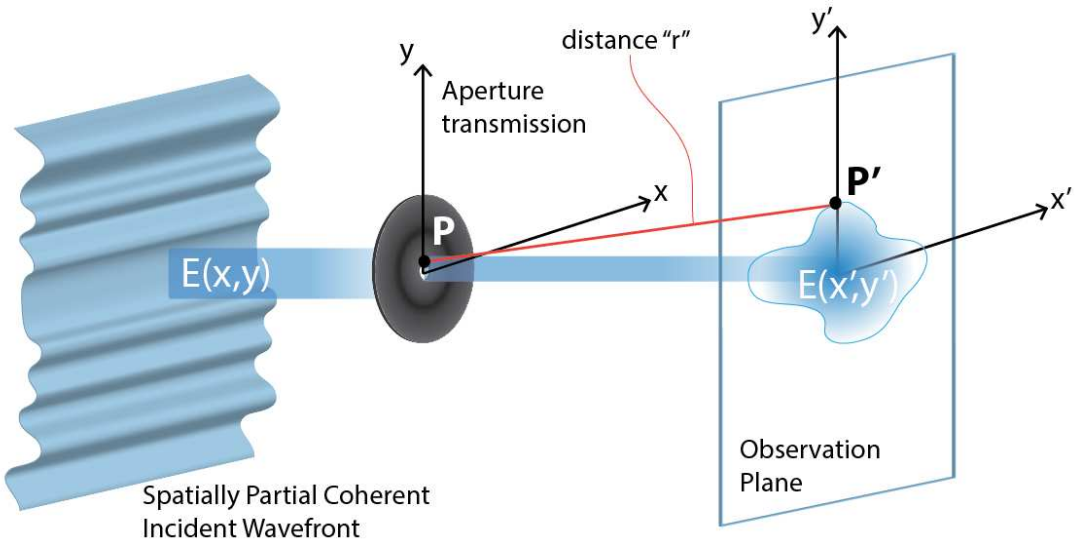

Figure 2.2: Diffraction of a spatially partial coherent light source from a circular aperture.

The field in the observation plane, E (x', y'), at point P' is given by a convolution:

$$E(x',y') = \iint h(x'-x, y'-y)t(x,y)E(x,y)dxdy \qquad \textbf{(2.16)}$$

As Huygens' Principle says that every point along a wave front emits a spherical wave that interferes with all others[17], here $h(r) = \frac{1}{i\lambda}\frac{exp(ikr)}{r}$ defines the spherical wave and as can be seen from Figure 2.2 r is the distance from P to P' and is equal to $r = \sqrt{(x'-x)^2 + (y'-y)^2 + z^2}$, where t (x,y) is the aperture transmission function.

In the denominator of the expresiion for h(r), we can approximate r by z. But we can't approxi-mate r in the complex exponential function by z because it gets multiplied by k, which is big, so relatively small changes in r can make a big difference. However, we can write:

$$r = \sqrt{(x'-x)^2 + (y'-y)^2 + z^2} = z\sqrt{1 + (\frac{x'-x}{z})^2 + (\frac{y'-y}{z})^2} \qquad \textbf{(2.17)}$$

And if ε<<1, $\sqrt{1+\varepsilon} \approx 1 + {}^{\varepsilon}/_{2}$;

$$r \approx z\left[1+\frac{1}{2}\left(\frac{x'-x}{z}\right)^2+\frac{1}{2}\left(\frac{y'-y}{z}\right)^2\right]=z+\frac{(x'-x)^2}{2z}+\frac{(y'-y)^2}{2z} \quad \textbf{(2.18)}$$

This yield:

$$E(x',y')=\iint \frac{1}{i\lambda z} exp\left\{ik\left[z+\frac{(x'-x)^2}{2z}+\frac{(y'-y)^2}{2z}\right]\right\} t(x,y)E(x,y)dxdy \quad \textbf{(2.19)}$$

By simply multiplying out the squares;

$$E(x',y')=\iint \frac{1}{i\lambda z} exp\left\{ik\left[z+\frac{(x^2-2xx'+x'^2)}{2z}+\frac{(y^2-2yy'+y'^2)}{2z}\right]\right\} t(x,y)E(x,y)dxdy \quad \textbf{(2.20)}$$

and factoring out the quantities independent of x and y:

$$E(x',y')=\frac{\exp(ikz)}{i\lambda z}\exp\left[ik\frac{x'^2+y'^2}{2z}\right]\iint \exp\left\{ik\left[\frac{(-2xx'-2yy')}{2z}+\frac{(x^2+y^2)}{2z}\right]\right\} t(x,y)E(x,y)dxdy \quad \textbf{(2.21)}$$

we can obtain equation 2.21, which is the Fresnel integral. It yields the light wave field E (x', y') after passing the aperture at the distance z from the screen in the cartesian coordinates. Same equation can be converted into cylindrical coordinates as[24]:

$$E(r,z)=-i\frac{exp\left[ikz+\frac{ik}{2z}r^2\right]}{\lambda z}\int exp\left(\frac{ik}{2z}r'^2\right)E(r')J_0\left(\frac{krr'}{z}\right)r'dr' \quad \textbf{(2.22)}$$

2.3.Partial Coherent Light Source Modelling in MATLAB

When modelling our partial spatial coherent light source we will now gather our results from section 2.1 and 2.2 into one equation.

In section 2.2, we get the insight to build the diffraction integrals and in section 1.4.2, we get even further by introducing this diffraction equation to a Gaussian beam. In the same section, we also introduced the phase of the axicon as an exponential as we shall remember again as below:

$$E(r,z)\propto \int exp\left(\frac{-r'^2}{{w_0}^2}\right).exp\left(ik\frac{r'^2}{2z}\right).exp(-ik_r r)J_0\left(\frac{krr'}{z}\right)r'dr' \quad \textbf{(2.25)}$$

Here now it is clear that first exp in the integral defines Gussian beam, second exp is its diffraction, third exp is the phase of axicon and rest is related to Bessel function.

In section 2.1, we found a phase from the superposition of many other waves. We have already defined the total phase as $\varphi_{incoh} = \sum_{i=1}^{n} \varphi_i$. This is the phase we will exponentialy add to our diffraction equation to also define the partial spatial coherency of our LED light source. Therefore, our final equation by taking into account all parameters would be:

$$E(r,z) \propto \int \exp\left(\frac{-r'^2}{{w_0}^2}\right).exp\left(ik\frac{r'^2}{2z}\right) .\exp(-ik_r r)\exp(-i\varphi_{incoh})J_0(\frac{krr'}{z})r'dr' \quad \textbf{(2.26)}$$

For all of the rest of the diffraction calculations, we will be considering the above-modeled 465 nm blue LED light source.

2.4. Numerical Calculations of Bessel Beams with Partial Coherent Inputs

After constructing the diffraction integral, considering the partial spatial coherent LED and the axicon, we get the calculation results on MATLAB. In our calculations, we have taken wavelength for the light source as 465 nm and put the tip angle of the axicon as 1°, just in our experiments. Because we want to see the affects of the degree of coherence (DOC) on our results, we have chosen the axial distance where calculations are performed as the focal length of the axicon. As we can see clear interference patterns here, we made sure that the altering affects would directly be connected to our changing of the DOC.

When modelling our partially spatially coherent light source we add a weighting factor to φ_{incoh}, related to the degree of coherence (DOC), by multiplying it with (1-DOC)

As the DOC closes to the value of one, the light source becomes more coherent. So we have calculated the transverse, longitudinal sections of the light wave fields and their diffraction patterns taking into account of different DOCs changing between one to zero. Results can be seen in the following figures.

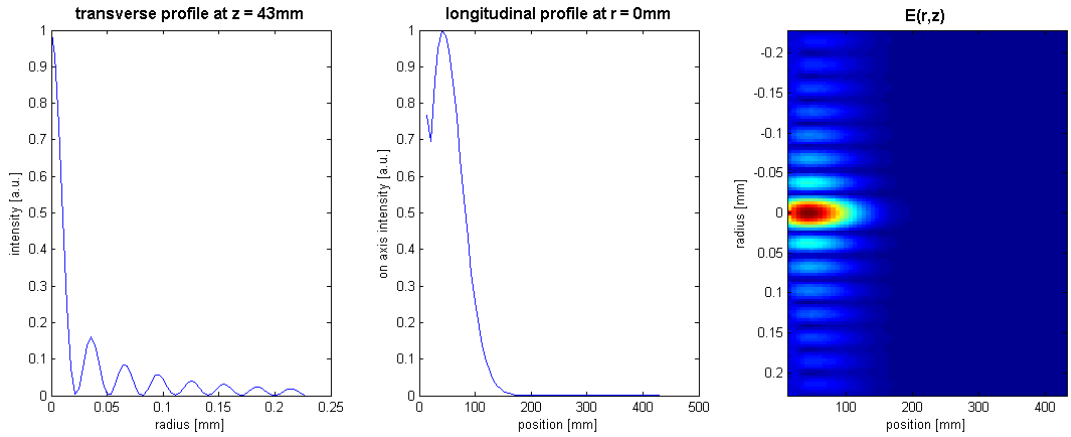

Figure 2.3: Diffraction results with DOC: 1

On Figure 2.3 with DOC:1, we have full coherence. This kind of calculation result isin good accordance with our experimets performed with lasers. The Bessel profile is very clear on the transverse profile, whereas we can observe a Gaussian like on axis intensity distribution on the longutidunal profile. Diffraction pattern can be seen on the right of the same figure.

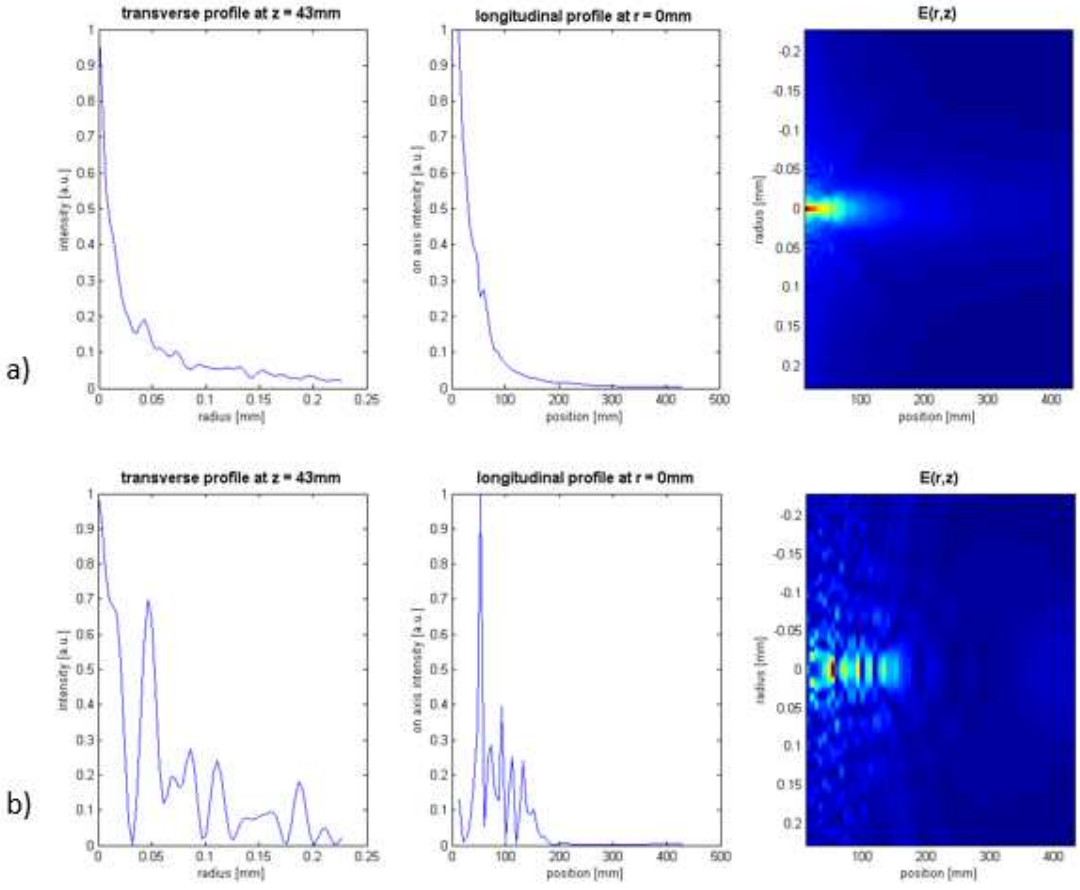

Figure 2.4: Diffraction results with DOC: 0.85

For all figures from 2.4 to 2.8, on part a) of the figures we see the average of 100 calculations where as on part b) we can see only one run from the calculations. As we have choosen random integers to calculate the incoherent phase coefficient, the avarage calculations has given more accurate results with that of the experiments as can be comparatively seen in each figure.

As in this figure, the DOC is 0.85, the coherence starts to decrease. So we see a clear deformation on the Bessel profile. However fringes are still appreciable and the on axis intensity profile is in good accordance with the experiments as the intensity gradually decreases after making a peak of intensity at the focal of aixcon. We can see the same affects at the diffraction pattern to the right of the same figure.

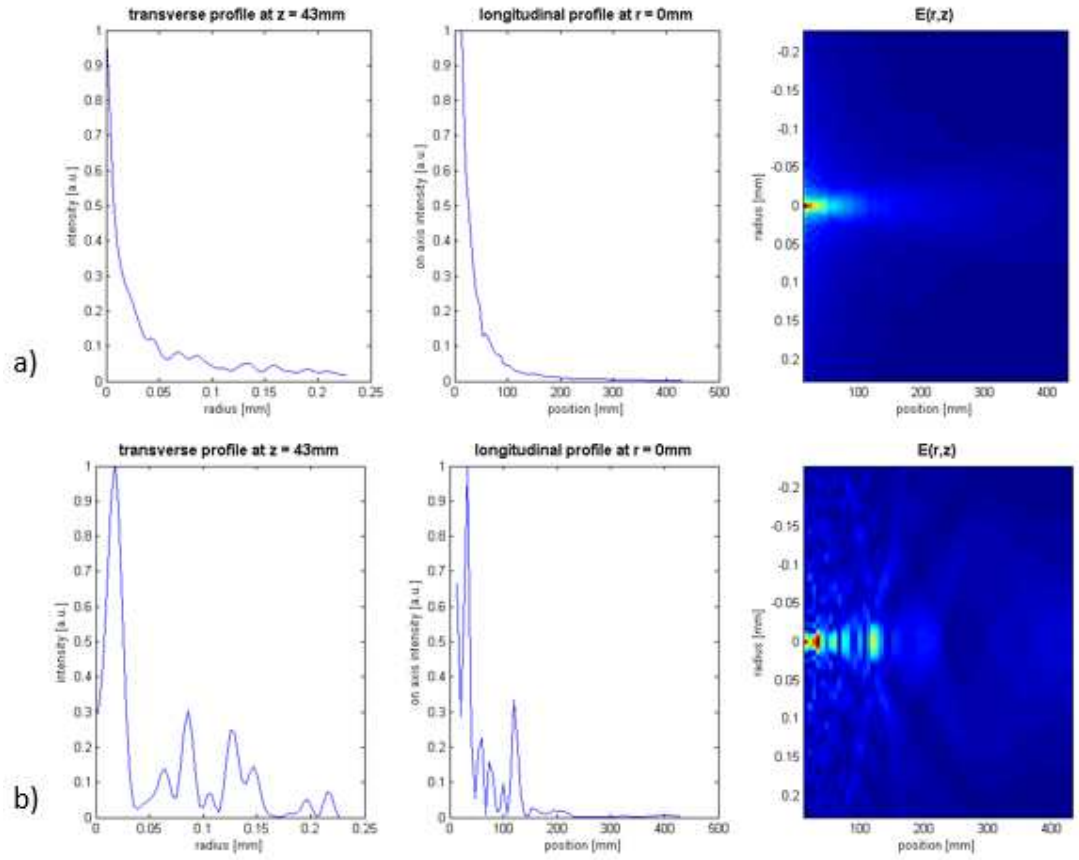

Figure 2.5: Diffraction results with DOC: 0.75

As we gradually decrease the degree of coherence down to 0.75 on Figure 2.5, we see that the peaks of fringes still remains however the clarity of them are not good as the DOC:0.85 case. We can see on the longitudinal profile that the decrase of the intensity is more stepper. The same affect can also be observed in the diffracted electromagnetic field as the blue low intensity area is smaller.

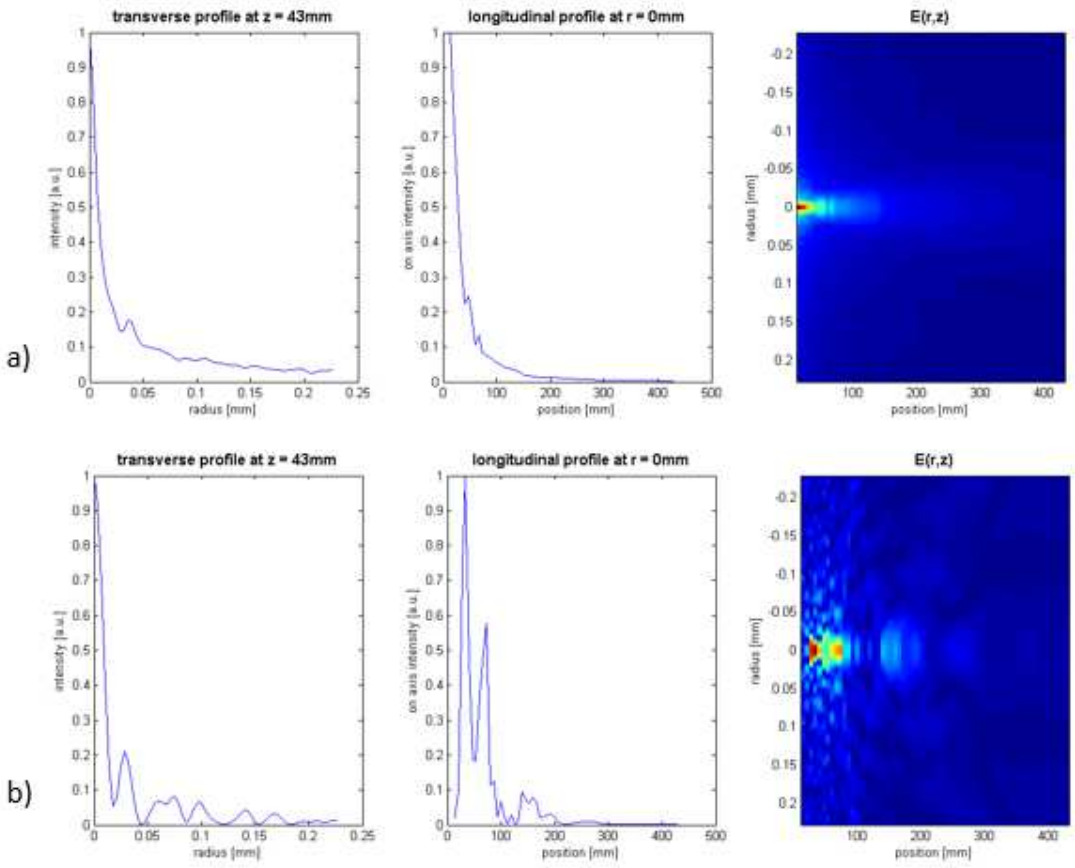

Figure 2.6: Diffraction results with DOC: 0.5

On Figure 2.6, we can realize that the peaks are more smoother on the transverse profile. The on axis intensity pattern again decreases gradually giving a similar profile to that of the results with DOC: 0.75. The diffracted field on the right is also giving similar distributions to that of the DOC:0.75 result.

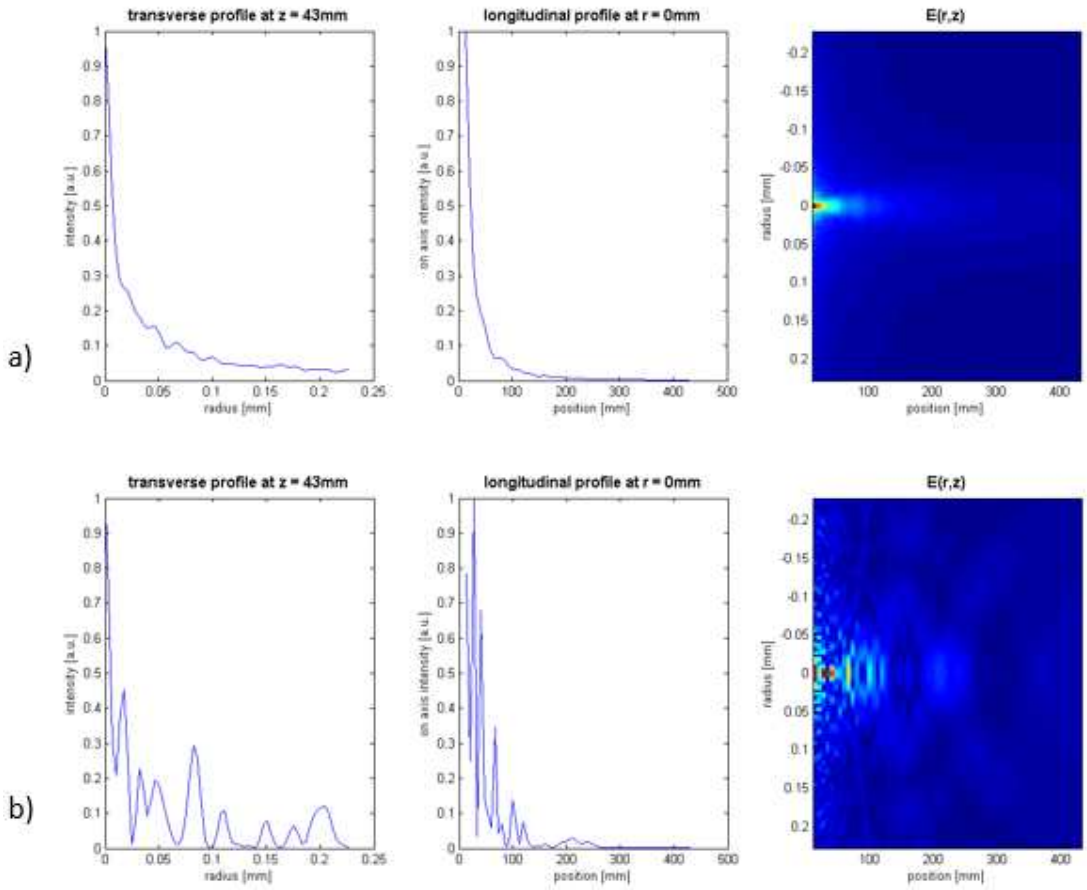

Figure 2.7: Diffraction results with DOC: 0.25

With DOC:0.25 on Figure 2.7, the transverse profile gets even more smoother. Here on the longitidunal profile we can see that the on axis intensity profile decreases even more stepper. We can read the same affects of decrease from the diffraction pattern to the right of the same figure.

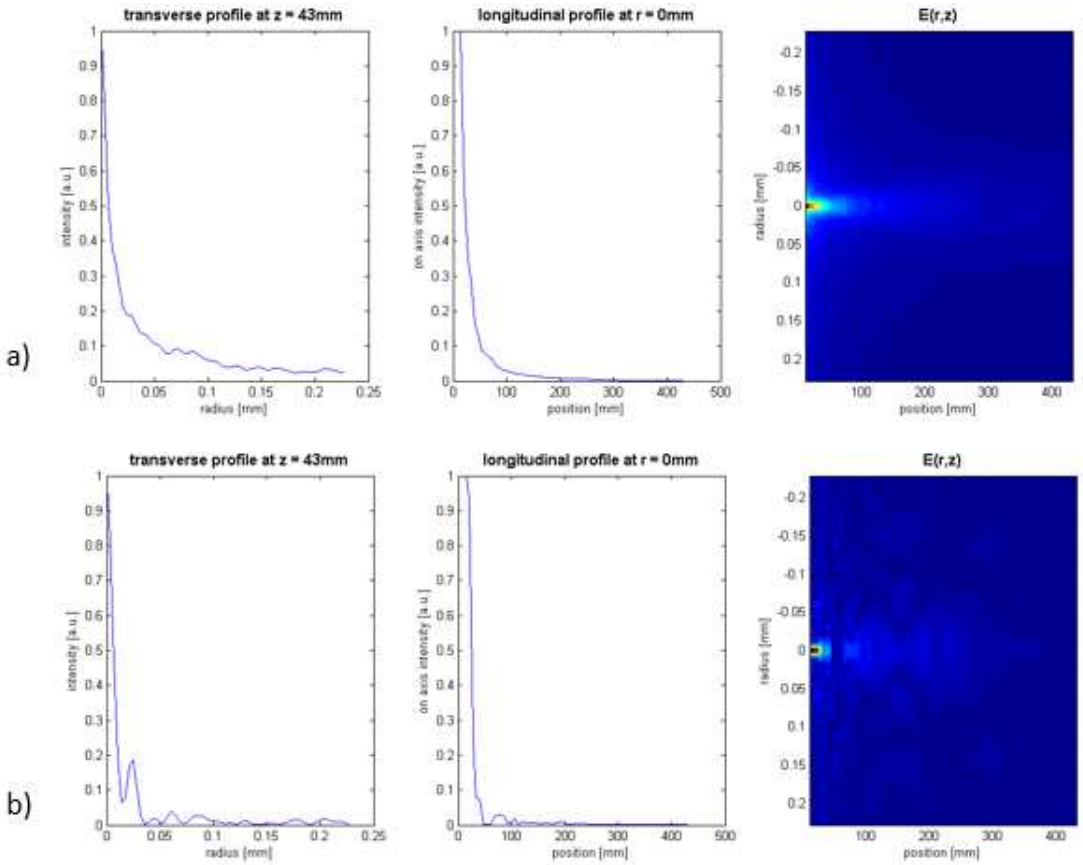

Figure 2.8: Diffraction results with DOC: 0

With DOC:0, our light source resembles an incoherent light source like a filamanted bulb. In this sense we loose the Bessel beam profile totally and the on axis intensity profile is steeper and the same affect is also observed on the diffracted electromagnetic field.

3.EXPERIMENTAL STUDIES with PARTIAL COHERENT LIGHT SOURCES

This chapter is opened to define our experimental set-ups, to declare our experimental findings and to give answers to our questions regarding the propagation dynamics of partial coherent light sources and their parameters. We generated both Bessel and Airy beams, so paid attention to define two main subsections for each beam and investigate each step one by one.

3.1 Bessel Beams

Generation and use of non-diffracting light beams is of increasing recent interest, for both fundamental and applied aspects[56]. In particular, Bessel beams formed by various approximate methods can exhibit quasi-diffraction-free propagation, as well as self-reconstruction over extended distances [57]. These beams are demonstrated to be enabling in a broad range of applications, such as plasma channel generation [58], optical particle manipulation [59] novel high-resolution optical microscopy techniques[60]and material processing [61, 62].

Fundamental studies, as well as applications of Bessel beams are performed predominantly with coherent (e.g. laser) sources. Indeed, the earliest theoretical works on diffraction-free propagation, by Durnin et al., are also based on monochromatic fields and plane-waves (with k-vectors distributed over surface of a cone) [39, 63]. As a result, high spatial and temporal coherence might seem to be prerequisites for Bessel beam formation.

On the other hand, questions remain about the relative importance of spatial and temporal degrees of coherence, as well as the consequences of partial coherence in Bessel beam generation. To this end, Fischer et al. investigated Bessel beams formed by white-light sources passing through an axicon, and concluded that temporal coherence is not of significant importance in the axial interference patterns **[64]**. They performed experiments with various sources with different spatial and temporal coherences, and observed the typical Bessel beam pattern in all cases, albeit with varying fringe numbers and visibilities.

Among these sources light-emitting diodes (LEDs) require further attention due to their intermediate spatial and temporal coherence and also rapidly growing practical use. Various types of LEDs are shown to be capable of forming Bessel beams **[65]**, the depth of non-diffracting zone being strongly dependent on the emitter profile. In a more extensive work, performances of LEDs and laser-type semiconductor sources (Lasers diodes or LDs) are compared **[66]**.

Detailed theoretical analysis of effects of coherence on diffraction-free propagation is performed by Bouchal and Perina **[67]**. Partial coherence is modeled by using superposition of plane-wave components with controlled angular correlation.

As the coherence decreases, lowest-order Bessel beams (with a central bright spot) exhibit broadening of the central lobe and smoothening of the fringe structure. For higher-order modes (i.e. optical vortices), incoherence fills the central null and destroys the vortex structure.

In this work, we present our comparative experimental work on formation of quasi non-diffracting beams by sources of varying temporal and spatial coherence. We particularly focus on propagation dynamics of these beams, i.e. investigate the beam profiles and the corresponding fringe visibilities as a function of propagation distance.

We observe that in addition to spatial coherence, the plane of observation is also critical to the observed beam profiles. In the case of a narrowband LED source, for example, high-quality Bessel-like beam in the Bessel zone progressively evolves into a light pipe with no fringe structure, at further propagation distances.

We perform experiments using a LD, a narrowband LED and a broadband LED. The sources represent high, partial and low spatial and temporal coherences, respectively.

We observe that the formation of Bessel beams is minimally affected by temporal coherence, consistent with observations in previous studies. On the other hand, we demonstrate that spatial coherence determines the evolution of the beam profile during propagation along the Bessel zone.

We first present a brief theoretical background and our experimental approach. We then present detailed experimental results on radial and longitudinal intensity profiles, observed with the three sources. Finally, we show quantitative analysis of fringe visibilities for each case.

3.1.1 Bessel Beam Formation Experimental Setup

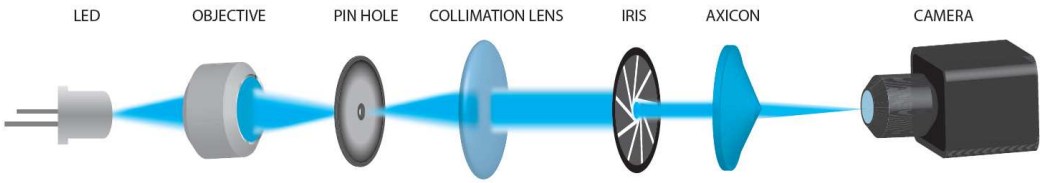

Figure 3.1: Experimental setup used for diffraction-free beam generation by incoherent sources[48].

The general layout of the experimental setup we used in our work is shown in Fig.3.1. As input light sources of different coherences, we used blue LED and white LED (phosphor type), as well as a red (633 nm) LD. The blue LED emits at 465 nm central wavelength. Due to its narrow bandwidth and small emitter area, the LED has a limited spatial and temporal coherence. In contrast, the phosphor-generated white LED source is highly incoherent. To collimate the light emitted from the source, we used a combination of a microscope objective with magnification of 30X, a pinhole with an aperture of 30 µm, and a positive lens. We used three different positive lenses with focal lengths of 15.4 mm, 50 mm, and 100 mm. Increasing the focal length of the collimation lens provides beams with larger diameters and longer Bessel zones., as well as larger coherence areas [66]. In order to limit the Bessel zone (for experimental ease), we adjusted the diameter of the input beam with an iris. The diameter of the beam was 5.3 mm for 100 mm collimation lens and 4.6 mm for other collimation lenses. To generate Bessel beam profiles, we used an axicon with a base angle of 1˚. In order to investigate the propagation behaviors, we recorded the images of the radial intensity profiles along the direction of propagation with a CCD camera (ThorLabs DCU223M), with pixel size of 4.65 µm.

3.1.2 Bessel Beam Experimental Findings

Figure 3.2 presents radial intensity profiles of the Bessel beams generated by the LD, with different collimating lenses. We recorded intensity profiles at a number of transverse planes. In the figure, each row corresponds to a given collimation lens (indicated in the figure title), while different columns show representative radial profiles from the beginning, middle, and end of Bessel zones, along the direction of propagation from the axicon. The last row shows two-dimensional beam profiles for these longitudinal positions.

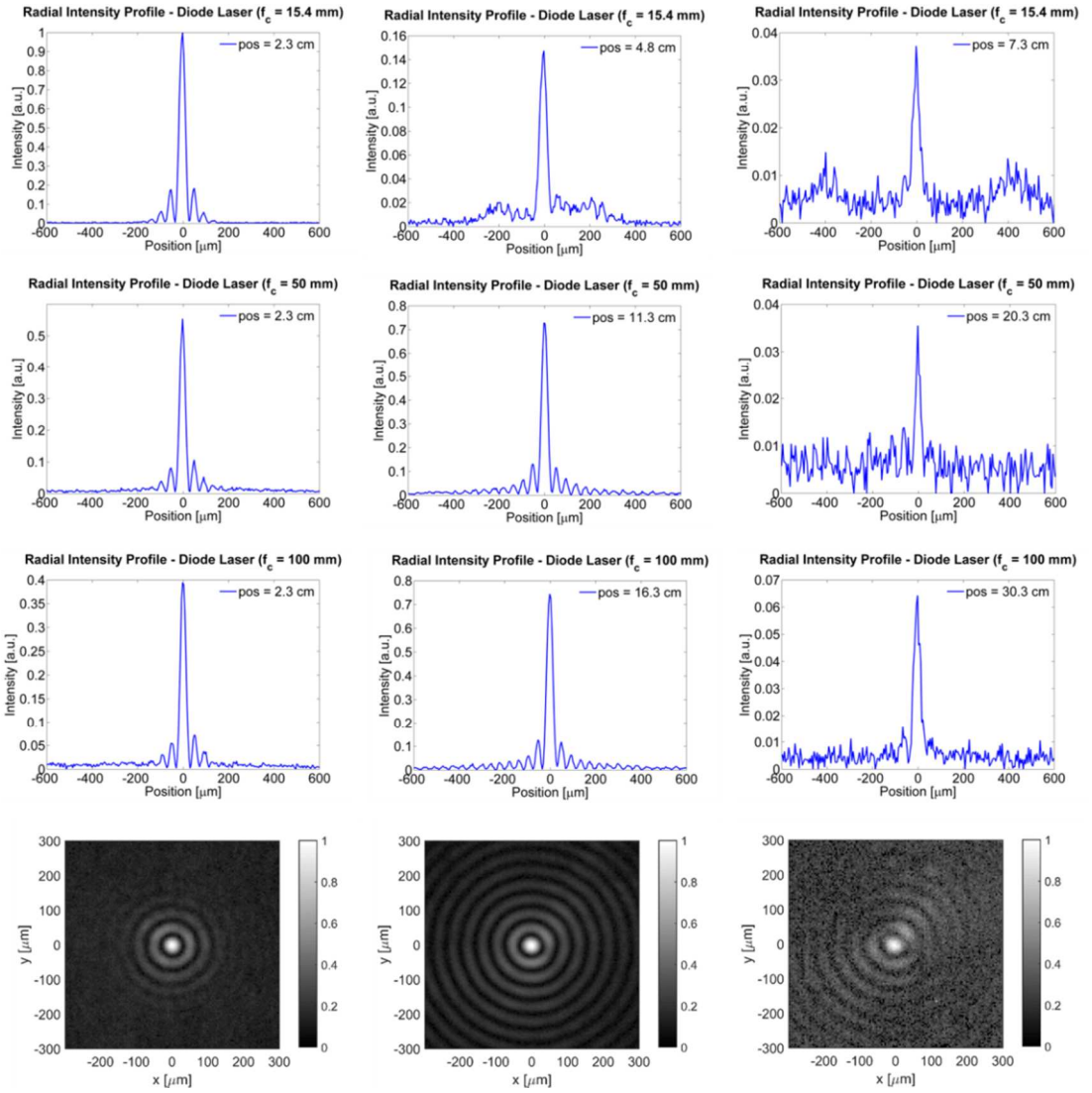

Figure 3.2: Profiles of Bessel beams formed by the diode laser[48].

The observations in this set of measurements are quite typical of Bessel-beam formation with a coherent source. The intensity profiles exhibit the expected Bessel-function-squared shapes, as long as the detection plane is within the Bessel zone. Only towards the end of the zone, the fringe structure start to disappear. In the case of 15.4 mm collimation lens, the zone ends earlier, due to smaller input beam size.

In the last row, images show the two-dimensional (2D) intensity profiles of the beams for 100 mm focal lengths of the collimation lenses. Square-root of the 2D data is taken for clarity of outer Bessel rings.

Lastly, it is also observed that the collimation lens has no direct effect on the contrast of fringes. Since the input is already highly spatially coherent, changing the beam diameter does not affect the coherence area to any significant degree.

The results of the same experiment done with Blue LED can be seen in Figure 3.3.

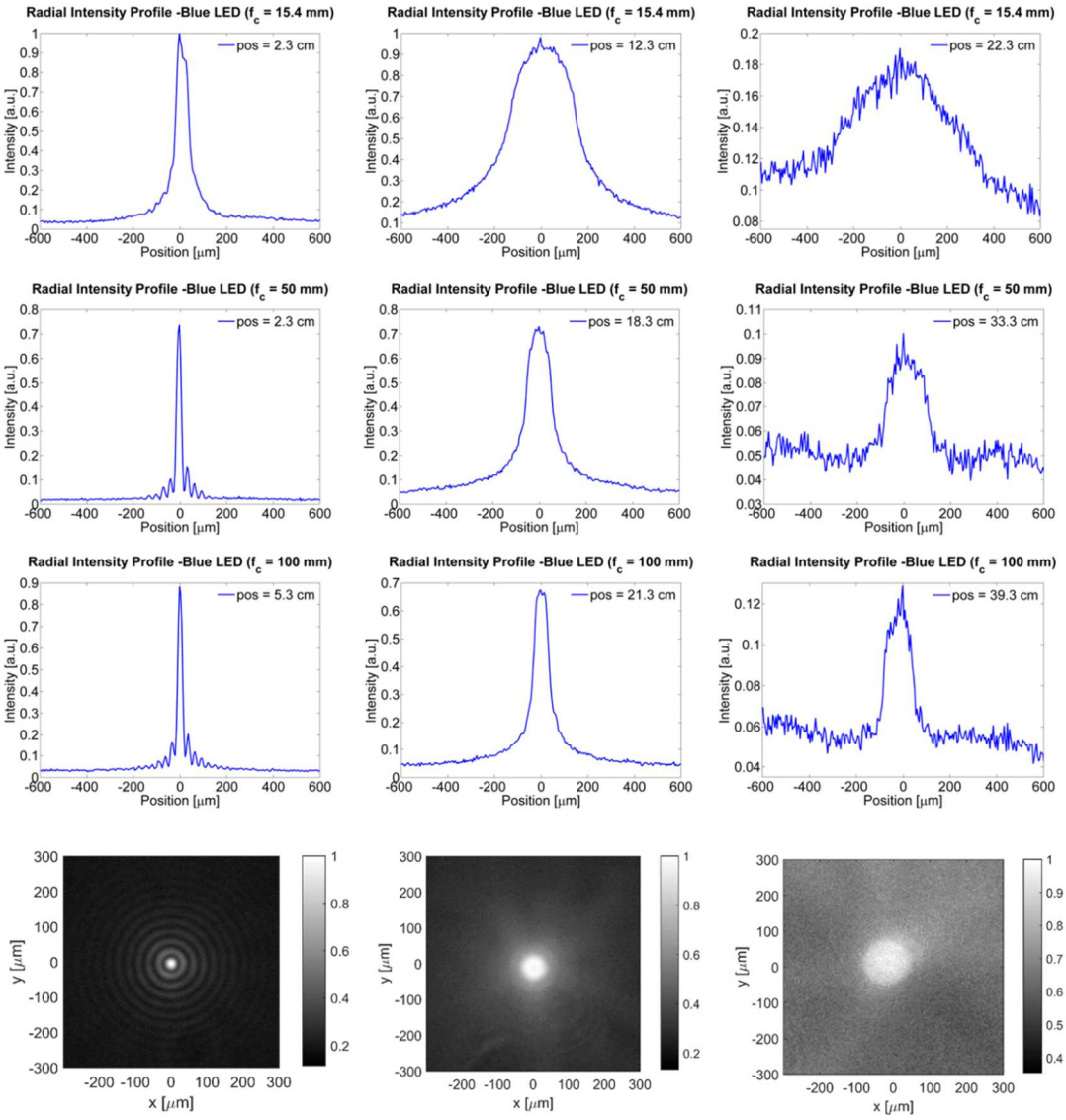

Figure 3.3: Profiles of Bessel beams formed by blue LED[48].

The experimental procedure for both of the LEDs is the same as the LD case. Figure 3.4 presents radial intensity profiles of the Bessel beams generated by using white LED. Number of important observations can be made with LED results, by noting that the spatial coherence area of the input increases with increasing the collimated beam diameter. For the smallest diameter (upper row), the Bessel-beam structure is completely absent. On the other hand, as coherence area increases the fringes start to appear, with a quality similar to the laser case (see below for more quantitative analysis). Furthermore, with a given coherence area, the Bessel beam structure is formed at the beginning of the Bessel zone, while the fringes disappear and the beam turns into a narrow cylindrical "light pipe" after some propagation. The diameter of the light pipe zone is smaller for higher degrees of coherence. This

observation is in accord with the theoretical predictions [67], and is further elaborated in the discussion section below.

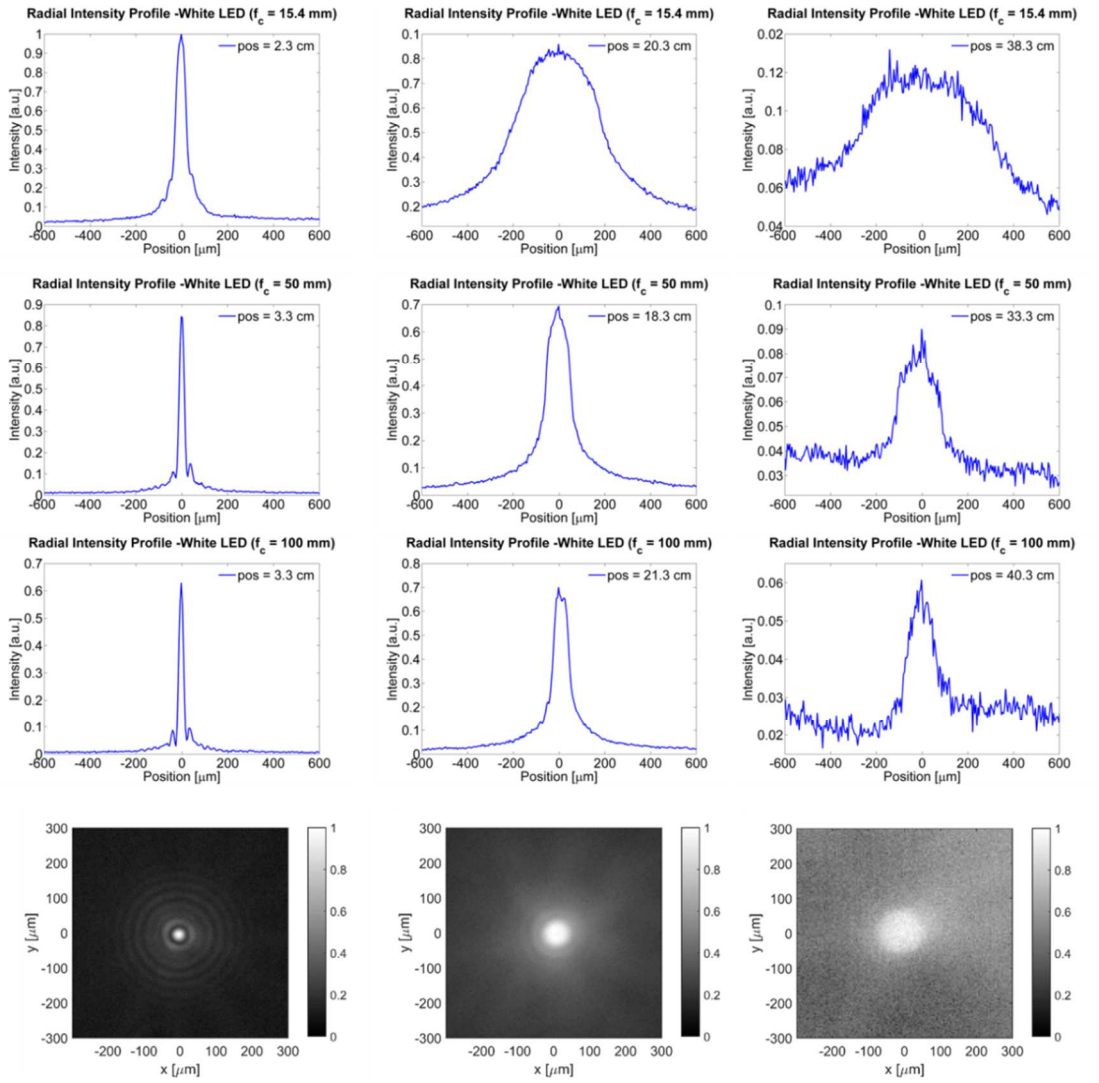

Figure 3.4: Profiles of Bessel beams formed by white LED[48].

The case of white LED, presented in Figure 3.4 is in general similar to the blue LED case. However, since the spatial coherence of the source is much weaker, the fringe contrast is lower and Bessel-like beams are observed over a narrower longitudinal range.

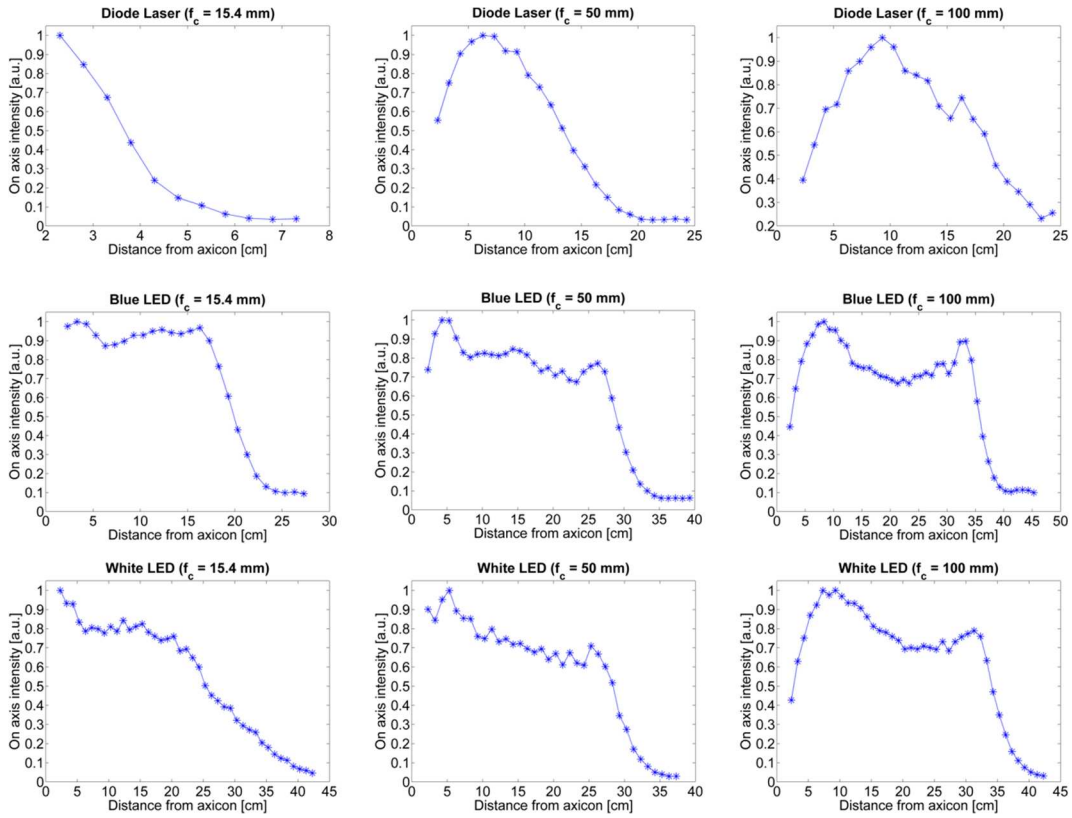

Figure 3.5: Propagation distance vs. on-axis intensity for the three different sources and collimation lenses[48].

Apart from the concentric-ring intensity patterns, another important property of diffraction-free beams is their extended high on-axis intensities. Hence, it is also important to compare the longitudinal evolution for the three different sources. Our measurements of on-axis intensities are shown in Figure 3.5. Columns (from left to right) correspond to 15.4 mm, 50 mm, and 100 mm focal lengths of collimation lenses. Rows (from top to bottom) correspond to different light sources of diode laser, blue LED and white LED.

The laser case follows the typical Gaussian-like (multiplied by propagation distance [42]) evolution. Both of the LED sources exhibit a more-uniform (nearly flat-top) intensity zones. In these cases, the inputs are not Gaussian, but rather rectangular beams, defined by the aperture of the iris. Therefore, the beginnings and ends of diffraction-free zones are steeper (smoothed out by diffraction).

In all cases, the length of diffraction-free zones increase with increasing input beam diameter, as expected from equation (1.21).

3.1.3 Bessel Beam Discussion

Bessel beam formation by axicon focusing provides intuitive way to understand the transverse intensity pattern. Waves coming from different parts of the input beam interfere constructively or destructively, depending on their relative phase. As a result, the transverse intensity profile is an interference pattern. On axis points, where all waves meet in phase and with largest amplitudes yield the highest intensity. When waves from two sources of partial mutual coherence overlap, the resulting intensity pattern will have maxima and minima given by**[24]**:

$$I_{max} = I_1 + I_2 + 2\sqrt{I_1 I_2} Re\{\gamma_{12}\} \quad \textbf{(3.1)}$$

$$I_{min} = I_1 + I_2 - 2\sqrt{I_1 I_2} Re\{\gamma_{12}\} \quad \textbf{(3.2)}$$

where $\boldsymbol{I_1}$and $\boldsymbol{I_2}$ are the intensities of incident waves, 'Re' denotes the real part and $\boldsymbol{\gamma_{12}}$ is the complex degree of coherence.

Since the effect of partial coherence is to reduce the fringe contrast, it is also logical to define visibility of the fringe structure, for the case of equal intensities as **[68]**:

$$V = \frac{I_{max} - I_{min}}{I_{max} + I_{min}} = |\gamma_{12}| \quad \textbf{(3.3)}$$

The amount of coherence can readily be measured by the interference visibility, which looks at the size of the interferenced fringes relative to the input waves.

As noted above, one of the most dramatic effects of the spatial coherence on the beam profile is to determine the fringe contrast. As a result, in order to make more quantitative discussions we measured fringe visibilities, as defined in equation (3.3). Since the intensity of the fringes decrease radially, we first divide the data with the envelope of the Bessel function[24], given:

$$f_{env} = |H[J_0^2(r) + Y_0^2(r)]| \quad \textbf{(3.4)}$$

where, the operator H generates complex-valued function with the real part same as the original data and the imaginary part given by its Hilbert transform. $J_0(r)$ and $Y_0(r)$ are the Bessel functions of the first and second kind respectively.

The procedure is outlined in the lower-left part of Figure 3. 6. We take average over 10 fringes around the center. The results are summarized in Figure 3.6.

With the laser beam, the visibilities are close to 1 at the central region of the Bessel-zone and decrease strongly before and after this zone. With the LED input, in general, visibilities are

typically well below the laser case. In addition, they rapidly fall towards zero by propagation. When the fringes disappear completely, the visibility is not calculated.

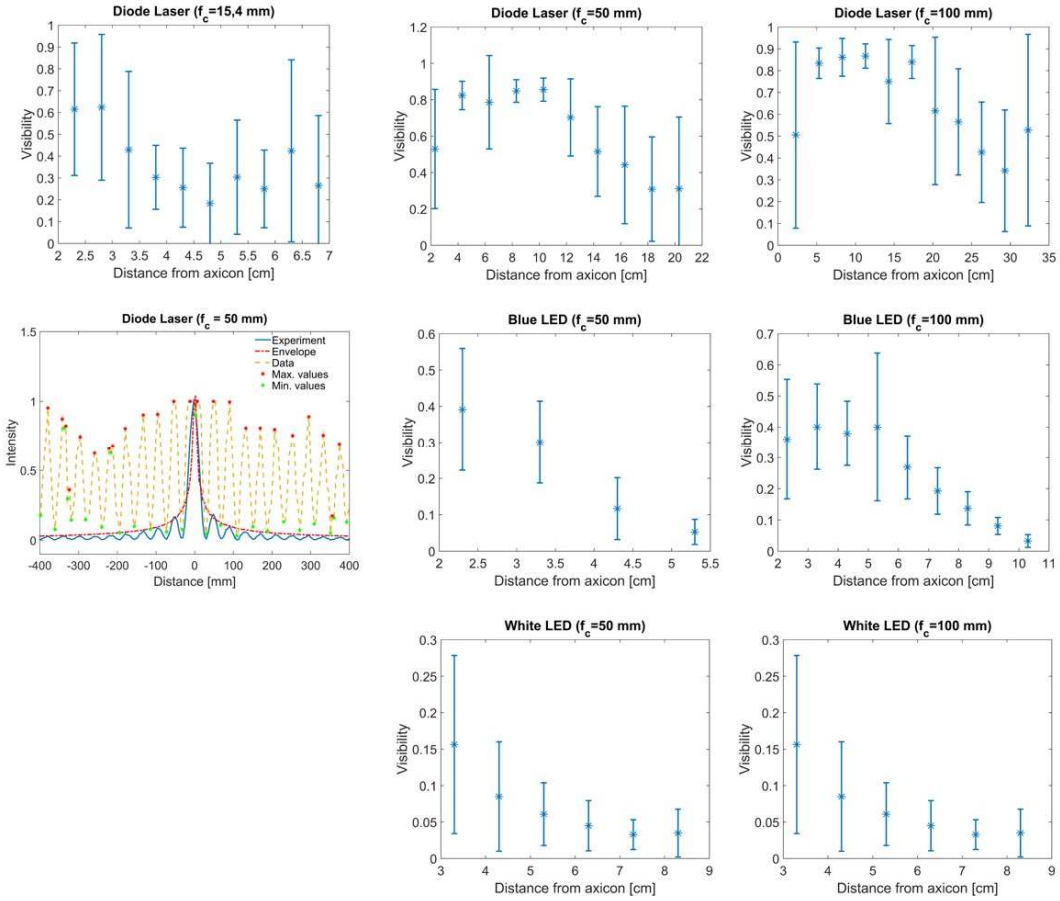

Figure 3.6: Propagation distance vs. visibility[48].

Columns (from left to right) correspond to 15.4 mm, 50 mm, and 100 mm focal lengths of collimation lenses. Rows (from top to bottom) correspond to different light sources of diode laser, blue LED and white LED. For the 15.4 mm case, the two LED sources yield no fringes, hence the visibilities are not calculated. Lower figure on the left column outlines the visibility calculation procedure.

The propagation dynamics of Bessel-like beams formed by incoherent sources can be understood by considering the interference picture outlined in Fig. 3.7. At a certain axial position behind the axicon, the radial profile is formed by superposition of waves incident on a finite area of the axicon. Sources like LEDs have a small, but finite coherence area, and when coherent waves from the small central region overlap (at the beginning of the Bessel zone), they exhibit interference effects. This is evident in the radial intensity patterns (Figures 3.3 and 3.4), as well as in the longitudinal intensities in the forms of a small peak at short distances. At longer distances, the overlapping waves come from outer regions of the input,

with low coherence relations. Hence, the interference structure disappears and what is observed as light pipe is simply addition of incoherent intensities.

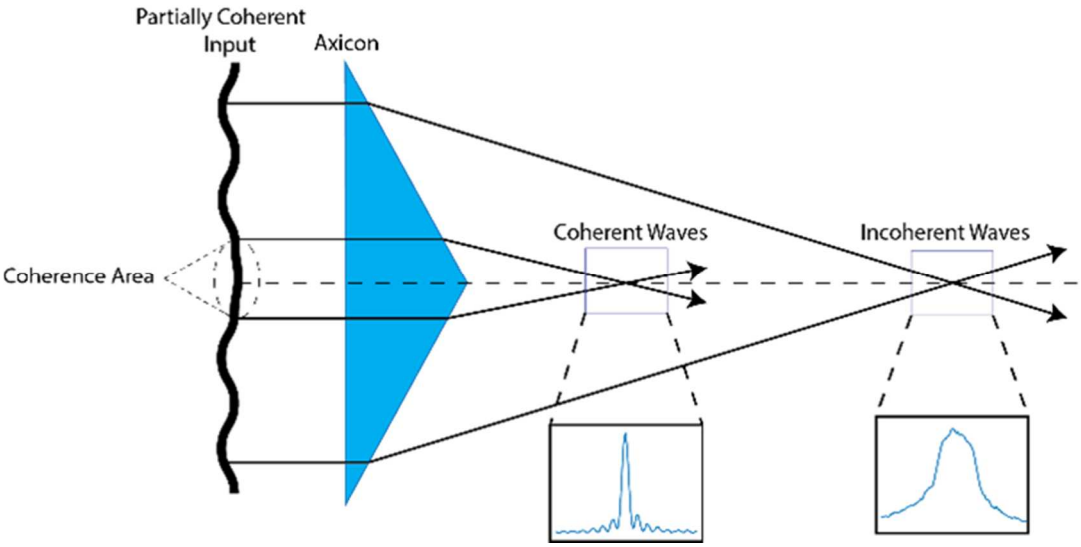

Figure 3.7: Schematic of the effect of spatial coherence on Bessel beam formation[48].

3.1.4 Comparison between Calculated and Experimented Bessel Beams

Here in this section we are focused on the comparative results between our experimental findings and the coded calculations. So first, we compared the transverse profiles at the distance 23mm from the axicon by taking the partial spatial coherent blue LED as the light source.

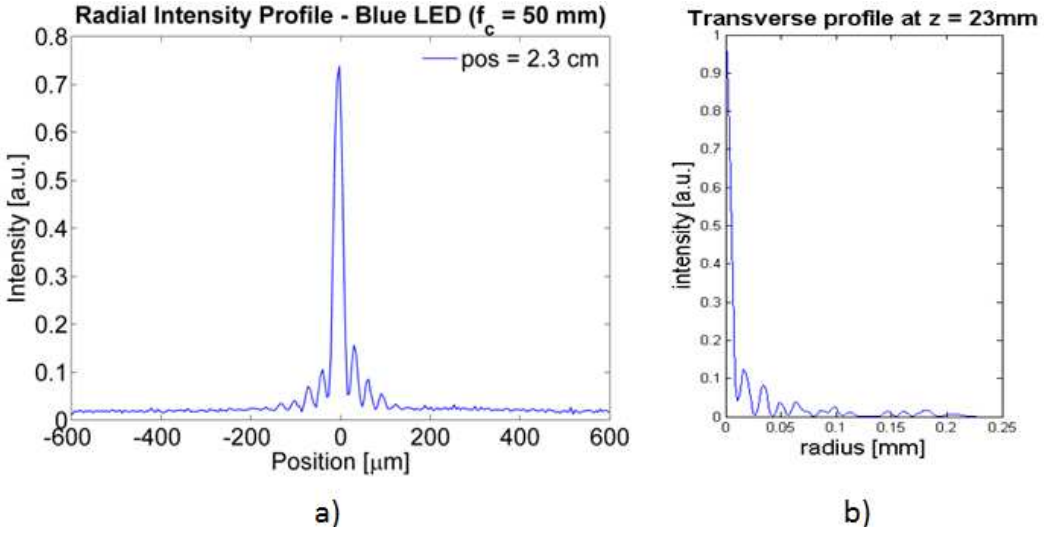

Figure 3.8: a) The experimental results at 2.3cm, b) the calculated results at 2.3 cm.

As can be seen on Figure 3.8 to the left we see a clear Bessel profile as we are on the focus of the axicon and the coherence of the interfering beams are high in that region. The same result can also be observed with the calculated beam profile on the right of the same figure.

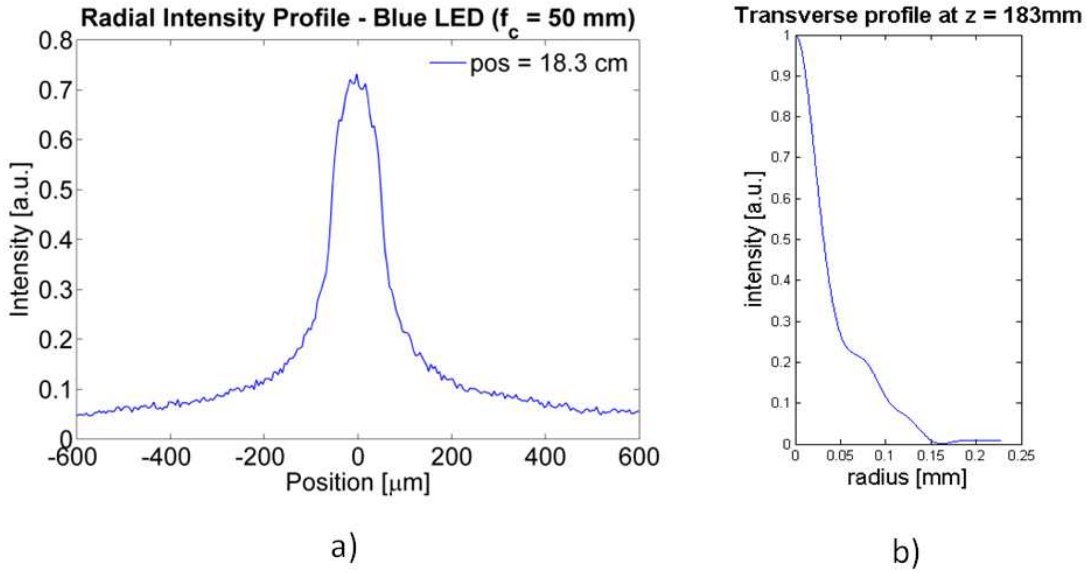

Figure 3.9: a) The experimental results at 18.3cm, b) the calculated results at 18.3 cm.

For Figures 3.9 and 3.10, we realize that the MATLAB modeled diffraction profiles on the rights are in good accordance with the experimented profiles on the left.

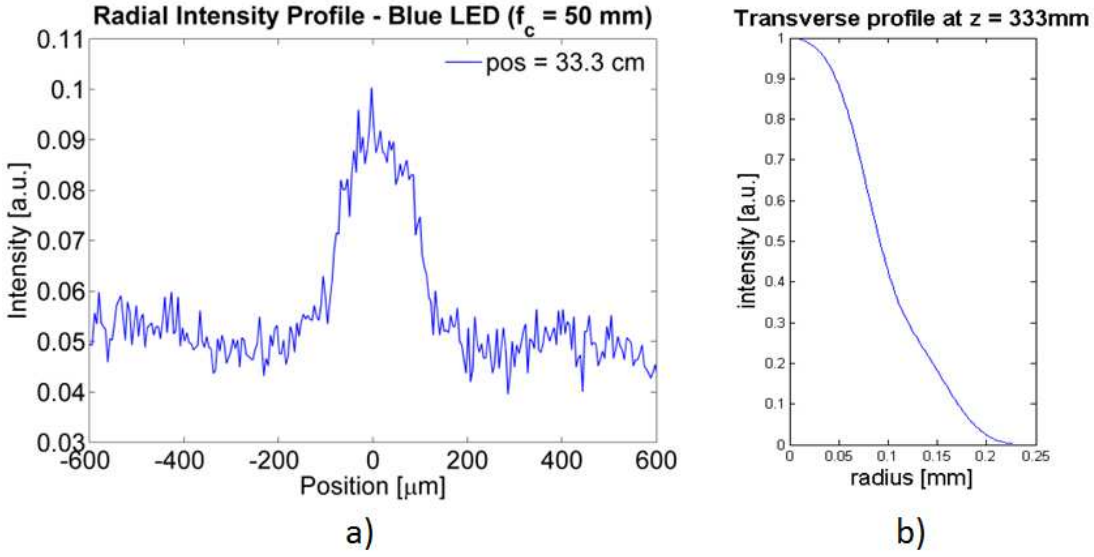

Figure 3.10: a) The experimental results at 33.3cm, b) the calculated results at 33.3 cm.

3.2 Airy Beam

Specially shaped light beams are receiving increasing attention from optics researchers, due to their exotic physical behaviors and potential applications [5]. As explained in the previous section, lots of study regarding Bessel beams are already done, Airy beams in this sensation has also great potential of research as they have even more characteristic properties. Differently from Bessel beams,however, Airy beams also exhibit “acceleration”[52]. We have already seen that Gaussian beams cen be converted to Airy-Gaus beams by introducing cubic spatial phase followed by Fourier transformation; recently it is also demonstrated that by using standard, inexpensive and readily available cylindrical lenses, a new optical element can be constructed for Airy beam formation [5]. The below Figure 3.11 resembles the idea of the Airy lens.

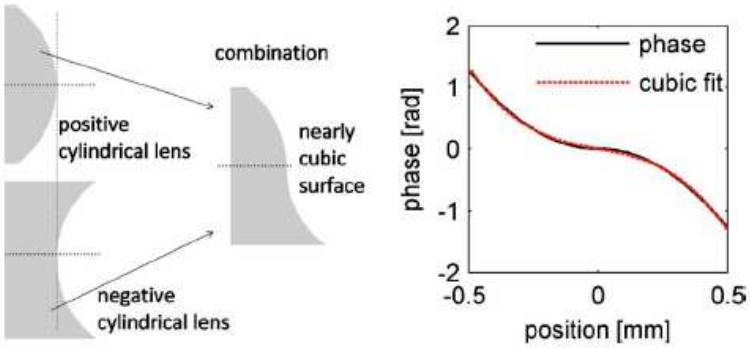

Figure 3.11: Construction of the Airy lens[5].

The basic idea in this lens is to match the actual phase delay caused by the optical element with a third order polynomial at the beam waist, $x = w_0$; as:

$$\frac{(n-1)kx^2}{2R} = \varphi_3 x^3 \qquad \textbf{(3.5)}$$

So that the coefficient of the cubic polynomial $\varphi_3 = \frac{(n-1)k}{2Rw_0}$ is defined where n is the index of refraction of the lens, k is the wavenumber, R is the radius of curvature of the convex side of the lens, w_0 is the beam radius (half-width at $1/e^2$ of the intensity), and φ_3 is the coefficient of the cubic polynomial.

3.2.1 Airy Beam Formation Experimental Set Up

When compared to laser, LED light source is more easily diffracted due to its initial partial coherency. That is why on the set up to generate airy beams we first used a convex lens to parallelize the beam coming from the iris.

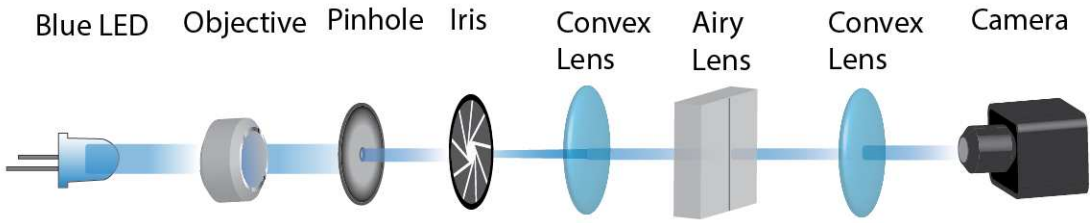

Figure 3.12: Set up of the Airy beam- blue LED experiment.

As can be seen from the Figure 3.12, we first have the blue led beam pass through an objective with a magnification ratio of 30. Then we focused the beam to a pinhole with 30 μm opening, we placed an iris to omit the noise and after to parallelize our beam used the first convex lens of 100mm foci. After the beam is parallelized we placed the airy lens, which gives the expected cubic phase to the beam.And after the airy lens, we used another convex lens of 125mm foci to give Fourier transformation to the beam. We placed the second Fourier lens exactly 125mm after the airy lens and expected to find airy beam profile at the focus. Just as expected we observed the clearest one dimensional airy beam profile on the foci of the Fourier transformation lens as can be seen on Figure 3.13.

3.2.2 Airy Beam Experimental Findings

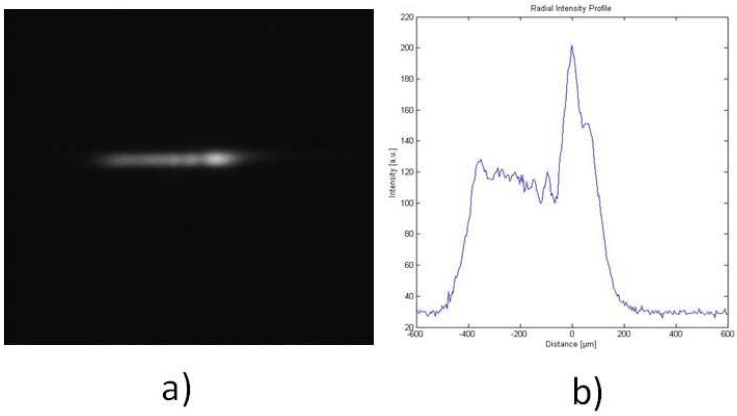

Figure 3.13: a)On the left experimeted Airy beam image on CCD camera , b) on the right Airy beam profile of the same image processed with MATLAB.

We measured radial intensity profiles changing with the distance and to measure the change in the beam profile we slide the usb ccd imaging camera on the ray and recorded measurement results via u Eye imaging program and processed the images via Mat lab. We also measured the gauss beams by removing the airy lens at the same set up to calculate the values of the bending we have. We measured max intensities via distance on the non-diffracting zone.

3.2.3 Airy Beam Discussions

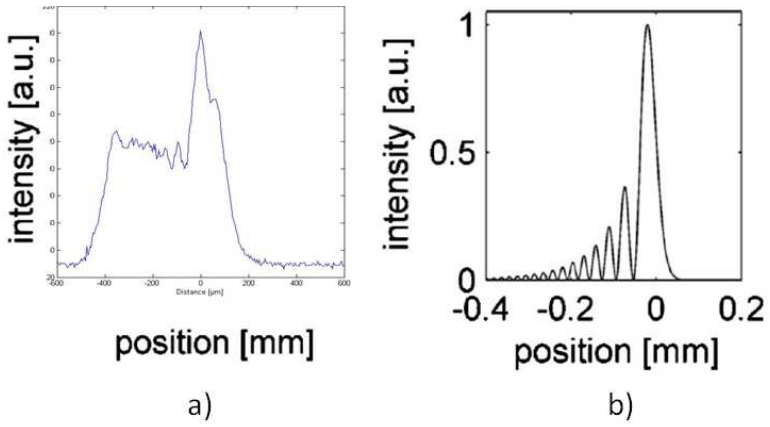

Figure 3.14: a) On the left LED generated experiment that we did, on the right laser generated experiment done by Yalızay et al. [5].

We can see from Figure 3.14 that as LED is more easily diffracted than laser the Airy beam profile is on the left is not in accordance with the one on the right. The same results can also be seen in the deflection profiles for each light source, we can see from Figure 3.15 that LED generrated deflection on the left is not in good accordance with laser generated on the right.

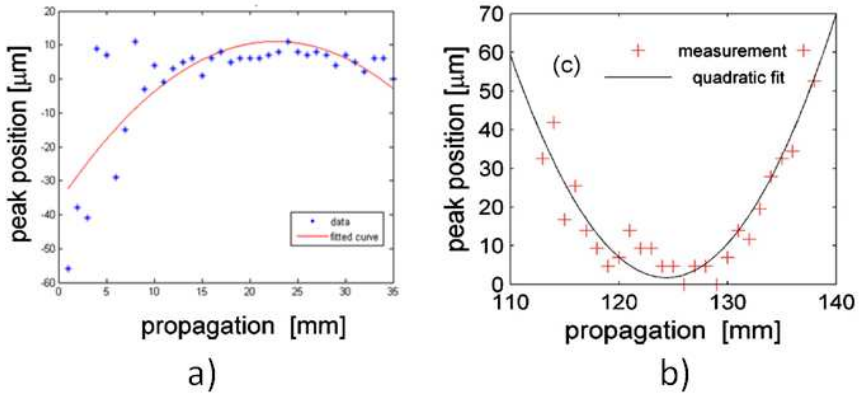

Figure 3.15: a) LED generated Airy beam's peak position-propagation profile b) laser generated Airy beam's peak position-propagation profile done by Yalızay et al[5].

So we can conclude that lasers are perfect light sources for airy beam application and LEDs are worth to investigate further with their similar optical characteristics to lasers. The Airy lens was a simple solution to integrate cubic spatial phase however, the profiles did not fit properly to the original Airy beam profiles generated with the same airy lens by using laser as the light source. Thus, we decided to investigate the advanced beam shaping parameters by using SLM with new experiments.

4. ADVANCED BEAM SHAPING WITH PARTIAL COHERENT LIGHT SOURCES

Airy beam profiles generated by using blue LED and Airy lens was not in good accordance with the profiles generated by using laser with the same set-up. This has evoked in us the will to further explore the LEDs by using a spatial light modulator (SLM). As SLM technology enables a more sensitive way to give spatial modulation to our initial light beam, we created this new section under the name of advanced beam shaping to further investigate the spatial properties of partial coherent ligh sources.

4.1 Spatial Light Modulator (SLM)

Spatial light modulator (SLM) is a general term describing devices that are used to modulate amplitude, phase, or polarization of light waves in space and time[69]. A simple example is an overhead projector transparency. In the 1980s, large SLMs were placed on overhead projectors to project computer monitor contents to the screen, since then projectors that are more modern have been developed where the SLM is built inside the projector [70].

Any desired light intensity distribution can be generated with high efficiency by controlling the diffraction and interference phenomena of light using light phase the modulation[71].

The use of LC materials in SLMs is based on their optical and electrical anisotropy.There are two basic types of SLMs; first is optically addressed SLMs(OASLM) which converts incoherent light to spatial modulation, second is electrically addressed SLMs(EASLM) which converts electrical signals to spatial modulation[72].

In our experiments we used HOLOEYE´s Spatial Light Modulator systems that are based on translucent (LCD) microdisplays[73]. The model of the HOLOEYE SLM that we used in our experimets is LC 2002 as can be seen in the Figure 4.1.

Figure 4.1 : LC 2002 model SLM that is used in our experiments[69]**.**

HOLOEYEs SLMs are based on either vertical-aligned nematic (VAN), parallel-aligned nematic (PAN) or twisted nematic (TN) microdisplay cells. In a twisted cell, the orientation of the molecules differs by typically 45°/90° between the top and the bottom of the LC cell and is arranged in a helix-like structure in between. In VAN / PAN cells the alignment layers are parallel to each other, so the LC molecules have the same orientation. The LC 2002 SLM contains Sony SVGA (800 x 600 pixels) liquid crystal microdisplay and drive electronics. The technical descriptions of the device are listed in the below table as:

Table 4.1: Technical properties of the LC 2002 SLM[73].

Description		**Units**
Outer package dimensions	82 (W) x 35 (H) x 23	mm
Active area dimensions	26,6 x 20,0 (1,3" diagonal)	mm
Screen aspect ratio	4 (H) : 3 (V)	
Display resolution	800 (H) x 600 (V)	pixels
Pixel pitch	32 x 32	µm
Pixel configuration	Orthogonal	
Gray Levels	256 (8 bit)	
Optical efficiency: transmittance	> 20	%
Aperture ratio	> 85	%
Optical Mode	translusive, monochrome	
Liquid crystal type	90° twisted nematic	
Polarizer Mode	Normally white	
Max. refresh frame rate	60	Hz
Illumination (max)	< 2	W/cm^2
Response time (typ.)	42	ms

The SLM can be used with a standard personal computer or laptop by plugging the device to a VGA graphics connector. The phase distribution of a beam incident on the SLM can be modulated by a voltage on the electrodes (800x600 pixels) of the LCD. The phase modulation is a side effect of the liquid crystal material and is caused by its birefringence property. By addressing electric pulse to the “pixels” to change the local electric field across the liquid layer, the pixels switch on or off[72].

It yields a more or less linear phase shift with voltage of maximum 2π radians at 532 nm. The SLM spatially carves the transverse profile of the beam and this can be usedin advanced beam shaping techniques like imaging, projection, display applications, holography, beam splitting, beam shaping, wavefront modulation, phase shifting, optical tweezers, pulse modulation. In order to use liquid crystal SLMs for gray-level phase control, a careful phase versus voltage calibration is required[74]. We will be explaining of our calibration steps in the following section.

4.2 SLM Calibration:

The calibration steps of the SLM has lead us to the further undertstanding of how the device spatially modulates the input light beam so we decided to include these steps as an additional section before directly explaining the advanced beam shaping experiments. For the calibration, the critical point was to find the appropriate degrees for both polarizer and analyzer. As these special optical elements are a kind of optical filter that passes light of a specific polarization and blocks waves of other polarizations, we defined different combination of degrees for both analyzer and polarizer. We tried to choose the best pair of degrees, when introducing the 2π phaseshift through our laptop. The experiment setup is shown in Figure 4.2.

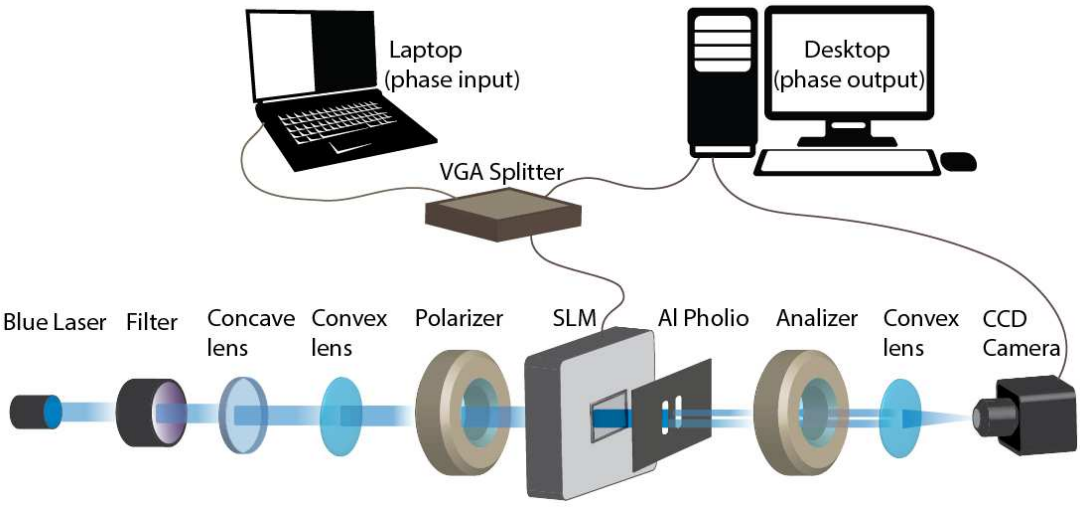

Figure 4.2 : The experiment set-up for calibration of the SLM.

For the calibration of SLM, the same blue laser that is used in the experiments of Bessel beam formation with the axicon is used to see clear phase shifts. It was

important for the diameter of the beam to cover the effective area of LCD so we used a telescope system composed of -50 mm concave and 400 mm convex lens to magnify the incoming beam by eight times. We used a metallic filter to not to exceed the maximum available value that we can detect in the CCD camera. The 0° position on the polarizer blocks horizontally polarized light and transmits vertically polarized components and as the orientation of the polarizer changes the polarization of the input beam to the SLM changes. After taking the spatial modulation from the device, the beam is splitted into two with an aluminium foil. The foil has 3 by 6 mm two holes with 1mm separation, which are opened by using a femtosecond laser. The splitted beam is then introduced to the analyzer. Two spllitted beams are then conveyed to a 200 mm convex lens to create interference in the focal plane of this lens and thus to have the fringe pattern. The voltage on the LCD pixels of SLM is proportional to the gray levels (0-255) of the image displayed on the laptop. A phase shift as a function of these addressed gray levels appeared as a shift in the interference pattern and we recorded the video of this shift by the Holoeye phasecam software. The “Start” button in the software starts the measurement and gray level from 0 to 255 is addressed onto the active half of the gray level window successively. An example of the addressed gray level pattern of the software and the corresponding changes in the fringe patterns can be seen in Figure 4.3.

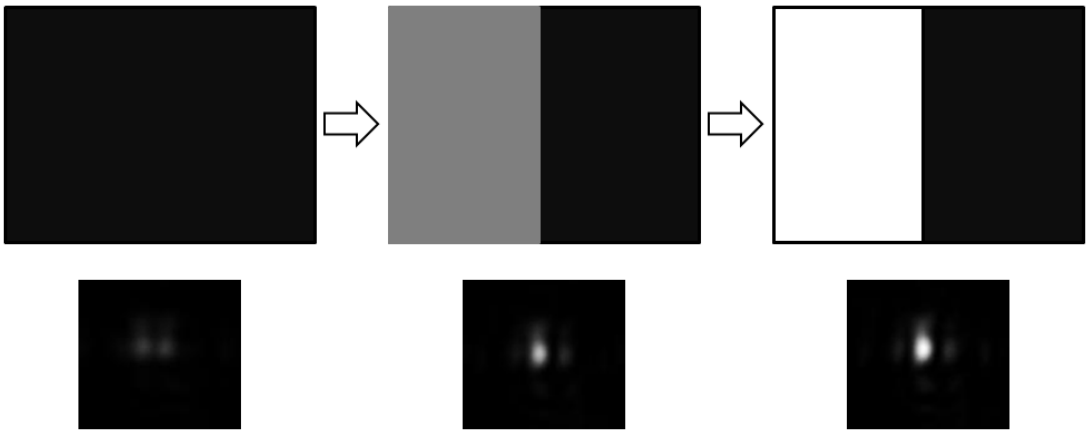

Figure 4.3 : Active gray level change pattern by the software and the corresponding change in fringe patterns.

We used blue laser as the light source to generate this 2π phase shift and recorded videos of the change in fringe patterns with different combinations of polarizer and analizor orientations. We have defined 300°, 315°, 330° rotations for polarizer and 0°, 15°, 30°, 45° rotations for the analyzer. To find the clearest 2π phase shift we have

analyzed each video. In order to do that, we have separated the videos into frames and find the maxiumum first three peaks in each interference pattern as can be seen in Figure 4.4. This procedure is done for every frame and afterwards all the peaks are sorted in an other graph to see how the phase shift affects the shift of the maximums of all first three peaks.

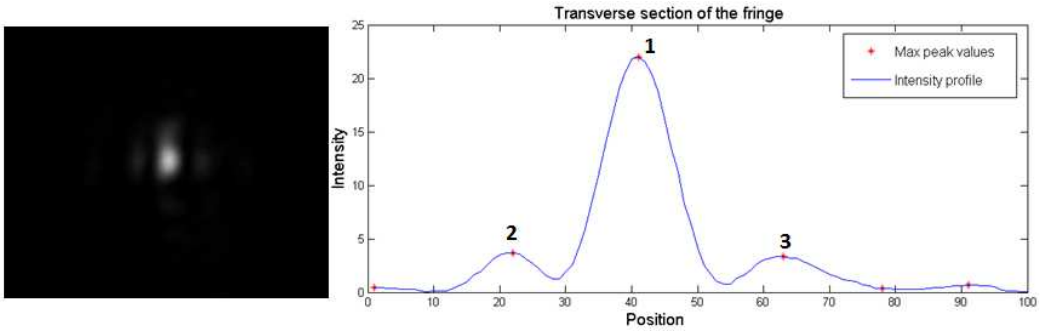

Figure 4.4 : An example of a fringe pattern and its transverse intensity section with maximum first three peaks.

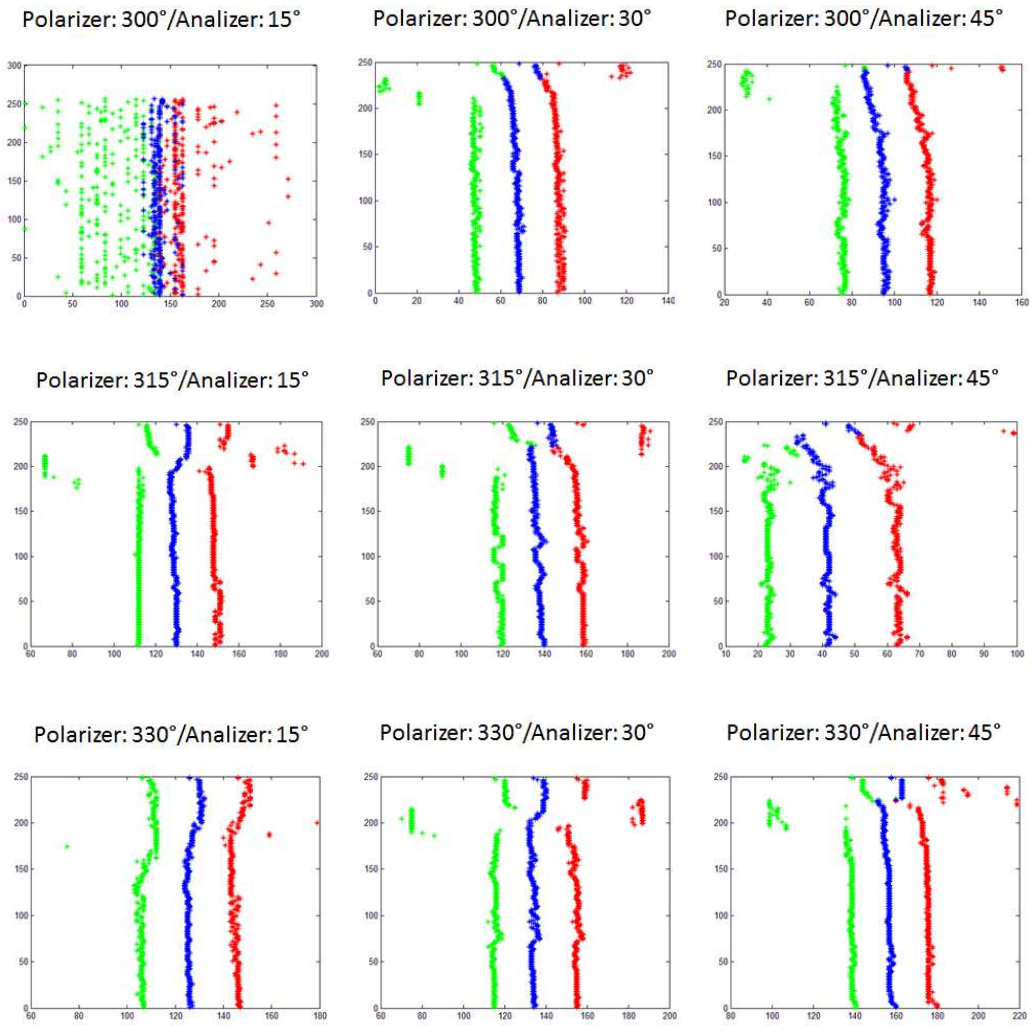

Figure 4.5 : Phase shifts for different combination degrees of polarizer and analizer.

Figure 4.5 shows the phase shifts of peaks for all type of degree combinations that are chosen for the polarizer and analizer. The vertical axis defines the number of frames for each video whereas the horizontal axis defines the intensity values for each peak. Here the blue lines shows the phase shifts for peak number one, green lines shows the phase shift for peak number two and red lines shows the phase shifts for peak number three. As a result the combination of degrees for polarizer: 315° and for analyzer: 45° has given the clearest phase shift. At this point we take the inverse of the 315°-45° graph and taken the polyfit of the central blue distribution as can be seen in Figure 4.6.

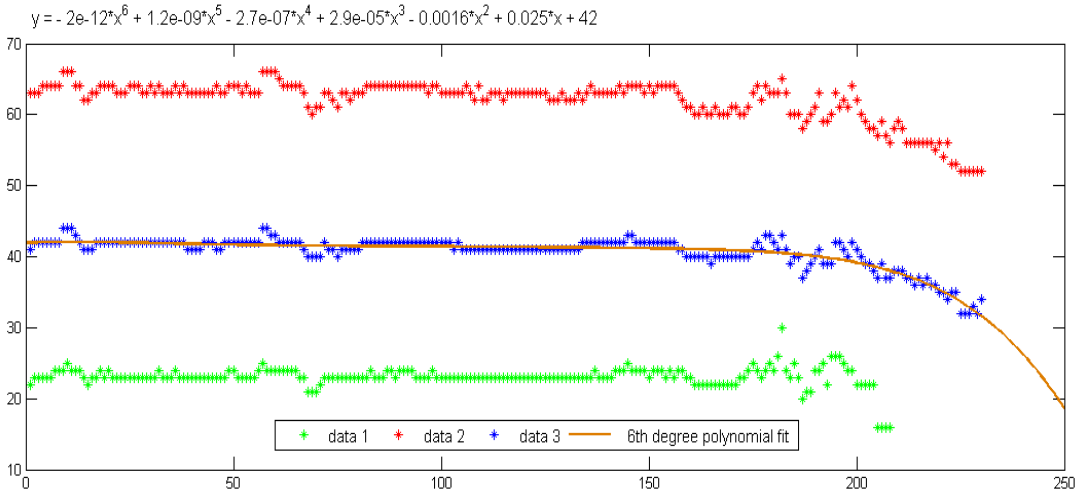

Figure 4.6 : Polyfit of the central peak values' distribution.

We have found the best accordance to the recorded data with sixth degree polynomial fit and the calculated phase is as below:

$$y = -2e^{-12}x^6 + 1.2e^{-09}x^5 - 2.7e^{-07}x^4 + 2.9e^{-05}x^3 - 0.0016x^2 + 0.025x + 42$$

We applied this inverted phase shift into every MATLAB code that is used for the rest of the experiments and made sure that SLM is calibrated.

4.3 Bessel Beam Shaping with SLM:

4.3.1 Experimental Setup:

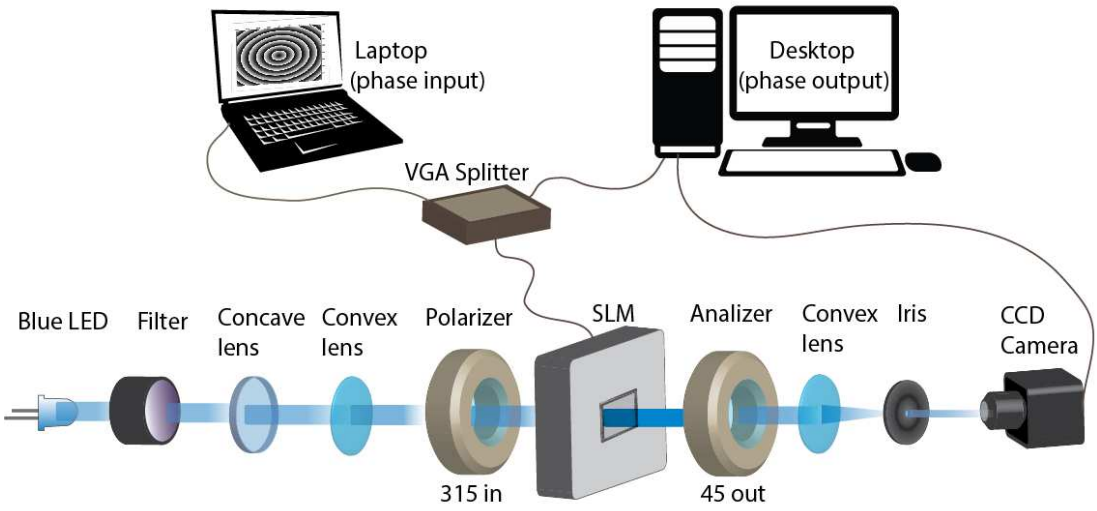

Figure 4.7 : The experimental set-up of the Bessel beam shaping with SLM.

Experiments for the formation of Bessel beams are done by both using the blue laser and blue LED which are used in the previous Bessel beam experiments that are done with the axicon. We have not concentrated on the change of the beam profile through the propagation axis as in the previous experiments done with axicon however; we have focused on searching for the potential formation of Bessel beams with partial coherent light sources. Blue laser in this perspective is just used for comparison with the previous Bessel beam experiment using an axicon.

As a difference from the calibration set up we took away the aluminium folio and so did not split the beam into two. The polarizer is set to 315° and analyzer to 45°. The collimating lens that is used after the analizer is a 100mm convex lens and iris is used to block the noise. Experimental findings are recorded by the CCD camera and conveyed to the desktop pc as the beam output.

4.3.2 Experimental Findings with Blue Laser:

As can be seen from the experimental set up on Figure 4.7 the phase input to the SLM is conveyed from the laptop with gray scale levels. We have coded the phase profile corresponding to Bessel beam on MATLAB, considering the refractive index, axicon tip angle, waveleght of the input light source. The axicon tip angle we used for this experiment was 0.1°.

We have used the calibrated phase of the polyfit we found and also introduced the Bessel beam phase. The resultant input phase can be seen on the left of the Figure 4.8 and the gathered intensity out put is observed by the CCD camera on the desktop pc as on the right of the same figure below.

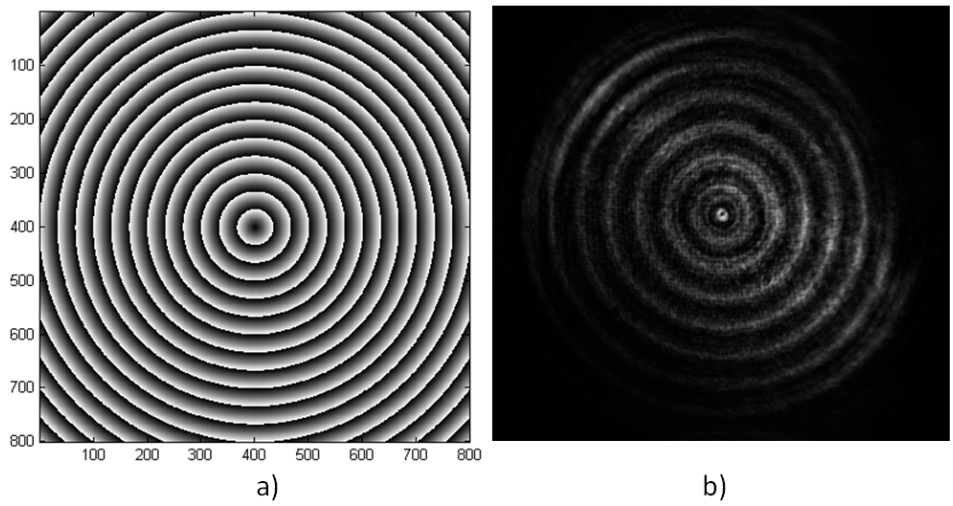

Figure 4.8 : a) The MATLAB coded Bessel profile,b) the observed Bessel profile by the CCD camera for blue lazer.

4.3.3 Experimental Findings with Blue LED:

The same procedure was repeated with that of the blue LED used in the before experiments. Once the phase profile corresponding to Bessel beam is sent to the SLM we got the final Bessel profile as seen on the right of the Figure 4.9. We have used the axicon tip angle as 0.02° as with this angle, we get the clearest beam profile.

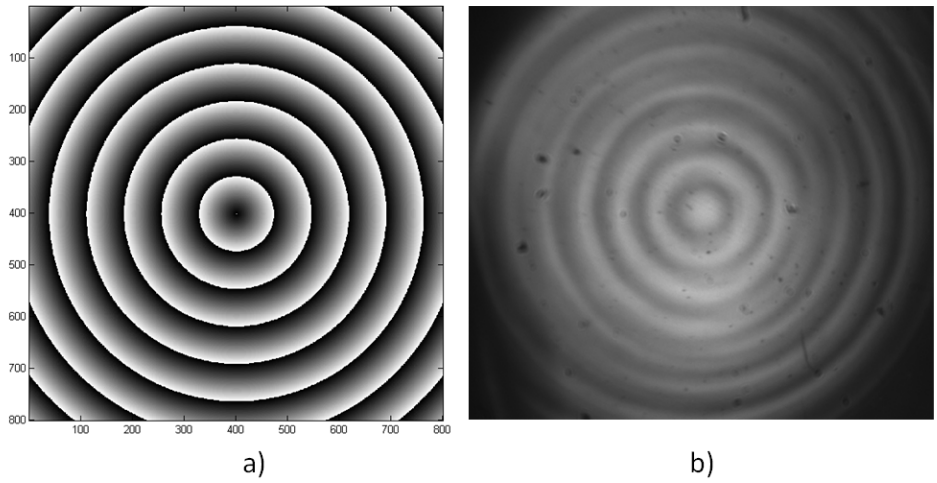

Figure 4.9 : a) The MATLAB coded Bessel profile,b) the observed Bessel profile by the CCD camera for blue LED.

4.3.4 Discussion:

One of the certain affects we have seen in the change of the observed beam profile was the change of the axicon tip angle. On Figure 4.10, we can see three different axicon tip angles and their MATLAB computed Bessel images, respectively.

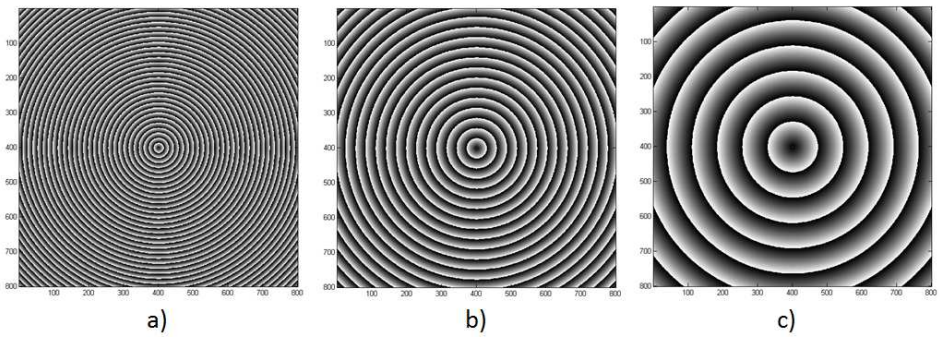

Figure 4.10 : a) The axicon degree of 0.1°,b) the axicon degree of 0.02° and c) the axicon degree of 0.05°.

One other difference that creates a major difference was the type of the light source that was used in the two experiments. We see that coherent laser source gives a sharp profile whereas partial coherent blue LED has given a more blended Bessel image due to its partial spatial coherence. The experimental findings has given parallel results with the basic beam shaping experiments done primarily.

4.4 Airy Beam Shaping with SLM:

4.4.1. Experimental Setup:

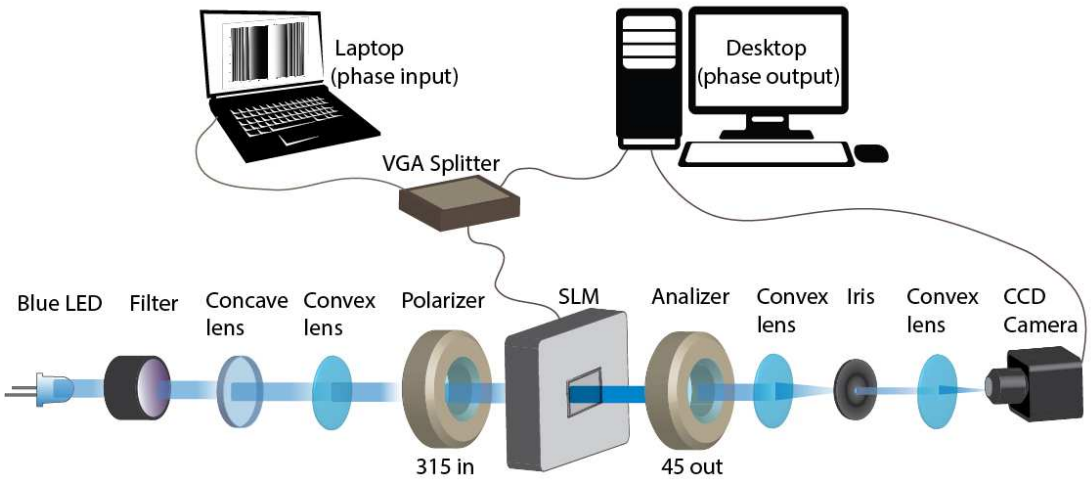

Figure 4.11 : The experimental set-up of the Airy beam shaping with SLM.

For the formation of the airy beam, we used the same telescope set up to magnify the beam 8 times as the width of the SLM. To do that we have used -50 mm concave and

400 mm convex lens. Polarizer and analyzer are set to the same orientation as in the calibration. The 50mm convex lens is used after the analyzer for collimating the beam, the iris is put to the focus of the 50 mm convex lens and it cancels the noise. The convex lens of 75 mm is put after the iris to the distance of 125 mm and it gives a fourier transformation to the beam and we finally can observe airy beam formations in our experimental findings.

4.4.2.Experimental Findings with Blue LED:

We have coded the Airy phase in MATLAB as can be seen on the left of the Figure 4.12. ,the resultant beam profile is observed 14mm away from the fourier lens as seen on the right of the same figure and the beam profile is not in accordance with the expected Airy beam profile.

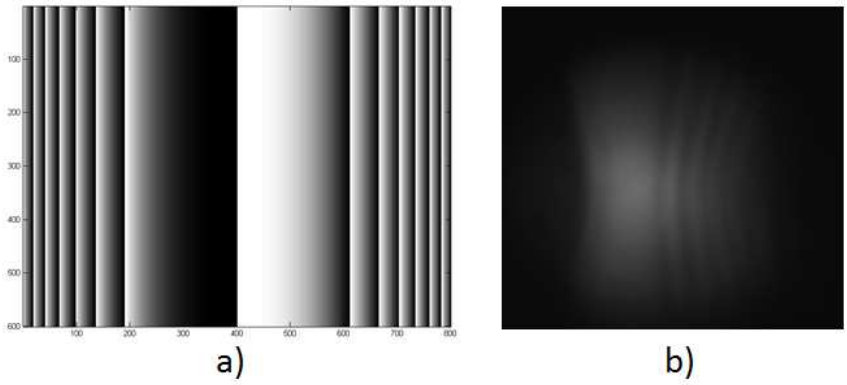

Figure 4.12 : a) The MATLAB coded Airy profile, b) the observed Airy profile by the CCD camera for blue LED.

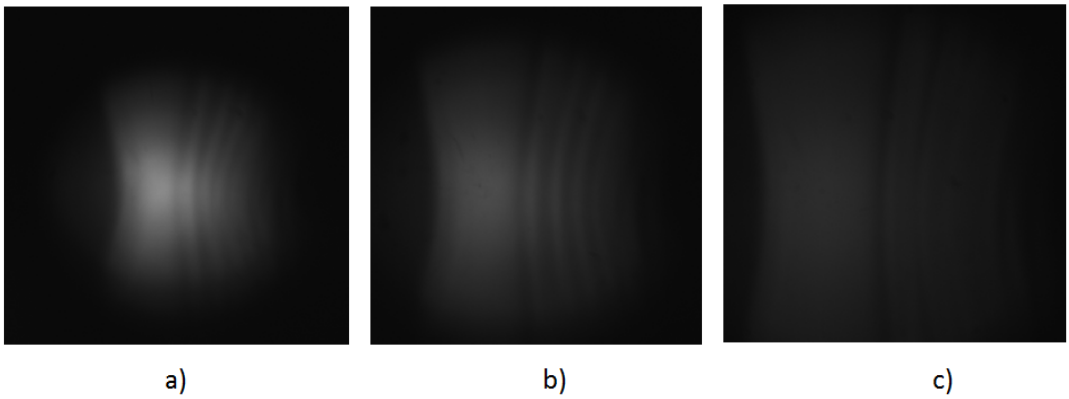

Figure 4.13 : Airy beam profiles at a) 14mm,b)15mm, c) 16mm away from the 75 mm collimation lens.

We can realize from the Figure 4.13 that the beam visibility gets less while the distance between Fourier lens and CCD camera increases.

4.4.3.Discussion:

One of the certain affects we have seen in the change of the observed beam profile was the change of the phase of the input beam by changing the exponantial degree of the Airy equation in our MATLAB code. The varying resultant phase inputs for the Airy beams is as in the following Figure 4.14.

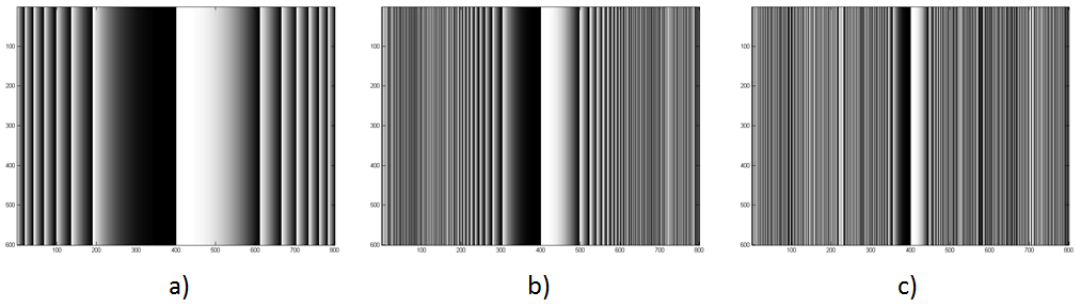

Figure 4.14 : a) The exponential degree: 7, b) the exponential degree: 8 and c) the exponential degree: 9, are seen as the differences in the phase input.

We can see that with partial spatial coherent light sources we cannot reach sharp beam profiles with expected Airy shifts. The beam visibility is easily lost and control over the beam profile is very limited. One of the certain reason for such affects is that SLM control techniques is very sensible compared to that of using optical elements like Airy lens. Mixing of diffraction orders due to array structure of SLM (32um pixel pitch) will create diffraction order that can wash out Beseel profile. On the other hand, translucent LCD structure might slightly diffuse transmission, reducing the contrast of the phase profile. In this regard due to Airy len's physical concrete structure, we get even better results with such optical element.

5. CONCLUSIONS AND PROSPECTS

We investigated propagation behaviors of two non-diffracting beams which are Bessel beams and Airy beams. These beams and their non-diffracting propagation had been already explored in the previous papers with lasers which are both temporally and spatially coherent so we give our attention to LEDs as they have varying spatial and temporal degrees of coherence.

When analyzing both beams' diffaction parameters, we observe that the temporal coherence is of minor concern as noted in previous works. On the other hand, the spatial coherence has determining role in the propagation dynamics within the diffraction-free zone.

For Bessel beams with high spatial coherence of the source, the concentric ring structure of the beam is observed throughout the zone. With sources of limited coherence, the intensity pattern depends not only on the coherence area of the input, but also on the observation plane. For Bessel beams almost in every case, it is possible to observe the Bessel profile in the near field, where the overlapping waves emerge from a small area (comparable to the coherence area). At longer distances, the fringe structure turns into a broad cylindrical light pipe. Lastly, in all cases, the on-axis intensity stays high over the entire diffraction-free zone.

For Airy beams we first used the Airy lens. Our results with the Airy lens by using LEDs has given a profile close the that of Airy beam. To be sure we also calculated the deflection of the maximum intensities through propagation. We have seen a parabolic trajectory very close to that of the deflection that was already detected in earlier papers by using Laser. As a further step, we decided to go further with advanced beam shaping experiments by using SLM. The calibration of SLM has given us important intuitive understanding of how to shape the spatial transverse profile of the incoming beam. We applied gray level as a phase input to generate Airy and Bessel images via SLM. We have found that Bessel profiles could not be clearly seen with SLM when compared to ones generated by axicon. The same result is accurate also for the Airy beams. Airy profiles has given more clear visibility with Airy lens rather than SLM. We have seen that just like Bessel beams, also the Airy profile strongly depends on the

coherence area of the input. We concluded the small coherence area to be an important reason for the insufficent wave profiles that we have detected. For further investigations we find it appropriate to scale the beam after it comes out of the pinhole so that a larger coherent area would be defined and more clear Airy profiles are expected to be seen. In this regard, LEDs with better temporal and spatial coherence degrees could be choosen for further experiments. And to the more SLMs with higher resolutions and reflective SLMs with smaller pixel pitch instead of the translucent device that we used in our experiment can be choosen.

In conclusion, our results show that spatially incoherent sources can be used in diffraction-free beam applications and depending on the particular goal, different longitudinal working planes could be selected to better serve the purpose. Moreover, the ability to spatially modulate partial coherent beams also creates great potential to carve the outcoming beam accordingly, paving the way to the new potential use and application of such sources.

REFERENCES

1. Mandel L, Wolf E (1995) Optical Coherence and Quantum Optics. Cambridge University Press

2. Ghatak A (2005) Optics. Tata McGraw-Hill Education

3. OXLasers OX-BL7 5 in 1 445nm 1000mW-1300mW adjustable burning blue laser pointer. http://www.oxlasers.com/sdp/925334/4/pd-4653056/10910768-2359907/OXLasers_OX-BL7_5_in_1_445nm_1000mW-1300mW_adjusta.html. Accessed 6 Jan 2016

4. Epistar LED Chip and Package from CNHidee LED Light Manufacturer. http://www.hideeled.com/en/news/Epistar-LED-Chip-and-Package-387.html#.Vo19M1JSJIg. Accessed 6 Jan 2016

5. Yalizay B, Soylu B, Akturk S (2010) Optical element for generation of accelerating Airy beams. J Opt Soc Am A 27:2344–2346. doi: 10.1364/JOSAA.27.002344

6. Sears FW (1946) Optics. Addison-Wesley

7. Hooke R (2005) MicrographiaSome Physiological Descriptions of Minute Bodies Made by Magnifying Glasses with Observations and Inquiries Thereupon.

8. Hecht E (2002) Optics, 4th ed. Addison-Wesley

9. Roychoudhuri C, Kracklauer AF, Creath K (2008) The Nature of Light: What is a Photon? CRC Press

10. Born M, Wolf E (1980) Basic properties of Elctromagnetic Fields. In: Wolf MB (ed) Principles of Optics (Sixth (Corrected) Edition). Pergamon, pp 1–70

11. Wolf E (2007) Introduction to the Theory of Coherence and Polarization of Light. Cambridge University Press

12. Hudgins WR, Meulenberg A, Penland RF (2013) A mechanism of wave interaction during interference. pp 883208–883208–13

13. Cowley JM (1995) Chapter 1 - Fresnel and Fraunhofer diffraction. In: Cowley JM (ed) Diffraction Physics (Third Revised Edition). North-Holland, Amsterdam, pp 3–24

14. Goodman JW (2015) Statistical Optics. John Wiley & Sons

15. Bertram D, Born M, Jüstel T (2012) Optics. In: Träger F (ed) Springer Handbook of Lasers and Optics. Springer Berlin Heidelberg, Berlin, Heidelberg, pp 623–640

16. Ball CJ (1971) Chapter 2- One dimensional Diffraction. In: Ball CJ (ed) An Introduction to the Theory of Diffraction. Pergamon, pp 12–39

17. Françon M (1966) Chapter 1 - Huygens' Principle and Diffraction Phenomena for a Monochromatic Point Source. In: Françon M (ed) Diffraction. Pergamon, pp 1–13

18. Françon M (1966) Chapter 5 - Extended Luminous Sources and Objects. Coherence. In: Françon M (ed) Diffraction. Pergamon, pp 53–97

19. Michelson AA (1920) On the Application of Interference Methods to Astronomical Measurements. The Astrophysical Journal 51:257. doi: 10.1086/142550

20. Selected Works of Emil Wolf (World Scientific). http://www.worldscientific.com/worldscibooks/10.1142/4331. Accessed 7 Nov 2015

21. Glauber RJ (1963) The Quantum Theory of Optical Coherence. Phys Rev 130:2529–2539. doi: 10.1103/PhysRev.130.2529

22. Elenbaas W (1972) Light Sources. Crane, Russak

23. Siegman AE (1986) Lasers. University Science Books

24. Principles of Optics : Max Born & Emil Wolf. In: Internet Archive. https://archive.org/details/PrinciplesOfOptics. Accessed 29 Apr 2015

25. Svelto O (2010) Principles of Lasers. Springer US, Boston, MA

26. Fox AG, Li T (1961) Resonant Modes in a Maser Interferometer. Bell System Technical Journal 40:453–488. doi: 10.1002/j.1538-7305.1961.tb01625.x

27. Paschotta R (2008) Field Guide to Lasers. SPIE, 1000 20th Street, Bellingham, WA 98227-0010 USA

28. Altingöz C (2014) Laser technology in automotive lighting. pp 896518–896518–11

29. Coaton JR, Cayless MA, Marsden AM (1997) Lamps and lighting. Arnold

30. Fowler, M. (2008) Black Body Radiation. In: Modern Physics. http://galileo.phys.virginia.edu/classes/252/black_body_radiation.html. Accessed 31 Oct 2015

31. 3 Watt Dimmable Filament LED E12 Candle Bulb. Edison Light Globes LLC

32. Nakamura S, Chichibu SF (2000) Introduction to Nitride Semiconductor Blue Lasers and Light Emitting Diodes. CRC Press

33. Ono YA (1995) Electroluminescent Displays. World Scientific

34. Sze SM, Ng KK (2006) Physics of Semiconductor Devices. John Wiley & Sons

35. LED diode. In: Fosilum. http://www.fosilum.si/en/why-led-lights/led-diode/. Accessed 3 Jan 2016

36. Nakamura S, Pearton S, Fasol G (2001) The Blue Laser Diode. Springer Berlin Heidelberg, Berlin, Heidelberg

37. Brandy, David Coherent optics and Holography. http://www.disp.duke.edu/~dbrady/ece469/notes/difffree/difffree.html. Accessed 10 Nov 2015

38. Durnin J (1987) Exact solutions for nondiffracting beams. I. The scalar theory. J Opt Soc Am A 4:651–654. doi: 10.1364/JOSAA.4.000651

39. Durnin J (1987) Exact solutions for nondiffracting beams. I. the scalar theory. J Opt Soc Am A 4:651–654.

40. McGloin D, Dholakia K (2005) Bessel beams: Diffraction in a new light. Contemporary Physics 46:15–28. doi: 10.1080/0010751042000275259

41. Lee,H.S., Stewart, B.W., Choi, K. (1994) Holographic nondiverging hollow beam. http://www.unboundmedicine.com/medline/citation/9910812/Holographic_nondiverging_hollow_beam_. Accessed 12 Nov 2015

42. Arlt J, Dholakia K (2000) Generation of high-order Bessel beams by use of an axicon. Opt Commun 177:297–301.

43. Indebetouw G (1989) Nondiffracting optical fields: some remarks on their analysis and synthesis. Journal of the Optical Society of America A 6:150. doi: 10.1364/JOSAA.6.000150

44. Mcleod JH (1954) The Axicon: A New Type of Optical Element. Journal of the Optical Society of America 44:592. doi: 10.1364/JOSA.44.000592

45. An In-Depth Look at Axicons | Edmund Optics. http://www.edmundoptics.com/technical-resources-center/optics/an-in-depth-look-at-axicons/. Accessed 3 Jan 2016

46. Lin Y, Seka W, Eberly JH, et al. (1992) Experimental investigation of Bessel beam characteristics. Applied Optics 31:2708. doi: 10.1364/AO.31.002708

47. McQueen CA, Arlt J, Dholakia K (1999) An experiment to study a “nondiffracting” light beam. American Journal of Physics 67:912–915. doi: 10.1119/1.19148

48. Altıngöz C, Yalızay B, Akturk S (2015) Propagation characteristics of Bessel beams generated by continuous, incoherent light sources. Journal of the Optical Society of America A 32:1567. doi: 10.1364/JOSAA.32.001567

49. Akturk S, Zhou B, Pasquiou B, et al. (2008) Intensity distribution around the focal regions of real axicons. Optics Communications 281:4240–4244. doi: 10.1016/j.optcom.2008.05.027

50. Berry MV, Balazs NL (1979) Nonspreading wave packets. American Journal of Physics 47:264–267. doi: 10.1119/1.11855

51. Siviloglou GA, Broky J, Dogariu A, Christodoulides DN (2007) Observation of Accelerating Airy Beams. Phys Rev Lett 99:213901. doi: 10.1103/PhysRevLett.99.213901

52. Siviloglou GA, Christodoulides DN (2007) Accelerating finite energy Airy beams. Opt Lett 32:979–981. doi: 10.1364/OL.32.000979

53. Polynkin P, Kolesik M, Moloney JV, et al. (2009) Curved Plasma Channel Generation Using Ultraintense Airy Beams. Science 324:229–232. doi: 10.1126/science.1169544

54. Schiff (1968) Quantum mechanics. McGraw-Hill Education (India) Pvt Limited

55. Bouchal Z, Wagner J, Chlup M (1998) Self-reconstruction of a distorted nondiffracting beam. Optics Communications 151:207–211. doi: 10.1016/S0030-4018(98)00085-6

56. Dholakia K (2008) Optics: Against the spread of the light. Nature 451:413–413. doi: 10.1038/451413a

57. Bouchal Z, Wagner J, Chlup M (1998) Self-reconstruction of a distorted nondiffracting beam. Opt Commun 151:207–211.

58. Polynkin P, Kolesik M, Roberts A, et al. (2008) Generation of extended plasma channels in air using femtosecond Bessel beams. Opt Express 16:15733–15740.

59. Paterson L, Papagiakoumou E, Milne G, et al. (2005) Light-induced cell separation in a tailored optical landscape. Appl Phys Lett 87:123901–3.

60. Chen Z, Taflove A, Backman V (2004) Photonic nanojet enhancement of backscattering of light by nanoparticles: a potential novel visible-light ultramicroscopy technique. Optics Express 12:1214. doi: 10.1364/OPEX.12.001214

61. Bhuyan MK, Courvoisier F, Lacourt PA, et al. (2010) High aspect ratio nanochannel machining using single shot femtosecond Bessel beams. Applied Physics Letters 97:081102. doi: 10.1063/1.3479419

62. Yalizay B, Ersoy T, Soylu B, Akturk S (2012) Fabrication of nanometer-size structures in metal thin films using femtosecond laser Bessel beams. Applied Physics Letters 100:031104–031104–3. doi: doi:10.1063/1.3678030

63. Durnin J, Miceli JJ, Eberly JH (1987) Diffraction-free beams. Phys Rev Lett 58:1499–1501.

64. Fischer P, Brown CTA, Morris JE, et al. (2005) White light propagation invariant beams. Optics Express 13:6657. doi: 10.1364/OPEX.13.006657

65. Sokolovskii GS, Dudelev VV, Losev SN, et al. (2008) Generation of propagation-invariant light beams from semiconductor light sources. Tech Phys Lett 34:1075–1078. doi: 10.1134/S1063785008120262

66. Sokolovskii GS, Dudelev VV, Losev SN, et al. (2014) Bessel beams from semiconductor light sources. Progress in Quantum Electronics 38:157–188. doi: 10.1016/j.pquantelec.2014.07.001

67. BOUCHAL Z, PEŘINA J (2002) Non-diffracting beams with controlled spatial coherence. Journal of Modern Optics 49:1673–1689. doi: 10.1080/09500340110114416

68. Thompson BJ (1965) Advantages and Problems of Coherence as Applied to Photographic Situations. Opt Eng 4:040107–040107–. doi: 10.1117/12.7971321

69. HOLOEYE Photonics AG » Spatial Light Modulators. http://holoeye.com/spatial-light-modulators/. Accessed 20 Nov 2015

70. (2015) Spatial light modulator. Wikipedia, the free encyclopedia

71. LCOS-SLM (Optical Phase Modulators) | Hamamatsu Photonics. http://www.hamamatsu.com/jp/en/4015.html. Accessed 20 Nov 2015

72. Hossack, Will (1998) Spatial Light Modulators and Applications. http://www2.ph.ed.ac.uk/~wjh/teaching/mo/slms.html. Accessed 21 Nov 2015

73. HOLOEYE Photonics AG » Discontinued Devices. http://holoeye.com/spatial-light-modulators/discontinued-devices/. Accessed 20 Nov 2015

74. Femtosecond pulse shaping using spatial light modulators. http://scitation.aip.org/content/aip/journal/rsi/71/5/10.1063/1.1150614. Accessed 21 Nov 2015

CURRICULUM VITAE

Name Surname: Ceren Altıngöz

Place and Date of Birth: Bursa, 23.03.1983

E-Mail: cerenaltingoz16@gmail.com

EDUCATION: Istanbul Technical University, Industrial Product Design (2006)

PROFESSIONAL EXPERIENCE AND REWARDS:

- Grouppe Renault, Lead Engineer (20 July 2015-still working)
- Magnetti Marelli Mako, Optics Engineer (19 July 2010-15 July 2015)
- Automotive Ligting France, Optics Engineer (August 2010- June 2011)
- SPIE scholarship (2014)
- Istanbul Technical University High Honour (2001-2006)

PUBLICATIONS, PRESENTATIONS AND PATENTS ON THE THESIS:

- Altıngöz, C., Yalızay, B., & Akturk, S. (2015). Propagation characteristics of Bessel beams generated by continuous, incoherent light sources. *Journal of the Optical Society of America A*, *32*(8), 1567. doi:10.1364/JOSAA.32.00156
- Altingöz, C. (2015). Airy wave packets and their application to automotive lighting. In K. P. Streubel, H. Jeon, L.-W. Tu, & M. Strassburg (Eds.), (p. 938304). doi:10.1117/12.2078359
- Altingöz, C. (2014). Laser technology in automotive lighting (Vol. 8965, pp. 896518–896518–11). doi:10.1117/12.2036519

OTHER PUBLICATIONS, PRESENTATIONS AND PATENTS:

- Altingoz,C.,(2013). Adaptive automotive lighting technology,9th National Illumination Conference
- Altingoz,C.,(2012). Led technology in Automotive lighting, 4th LED conference.
- Altingoz,C., Yalızay,B.,Akturk, S., (2014), Parabolik hüzmelerin otomotiv aydınlatmasında uygulamaları, Fotonik 2014, 16. Ulusal Optik, Elektro-Optik ve Fotonik Çalıştayı.